Herzig, P.M., Humphris, S.E., Miller, D.J., and Zierenberg, R.A. (Eds.), 1998
Proceedings of the Ocean Drilling Program, Scientific Results, Vol. 158

17. GEOCHEMISTRY OF BASALTIC ROCKS FROM THE TAG HYDROTHERMAL MOUND (26°08′N), MID-ATLANTIC RIDGE[1]

Susan E. Smith[2] and Susan E. Humphris[3]

ABSTRACT

Variably altered basalts, hydrothermal clays, and metabasaltic clasts were recovered during the Ocean Drilling Program (ODP) Leg 158 from the Trans-Atlantic Geotraverse (TAG) hydrothermal mound at 26°08′N, 44°49′W, on the Mid-Atlantic Ridge. These basaltic samples exhibit whole-rock chemical changes resulting from hydrothermal alteration of mid-ocean ridge basalt (MORB) at the edges of the TAG mound and within the stockwork zone. Relatively unaltered basalts are used to constrain the petrogenetic history of the magmas in the TAG region. The whole-rock compositions of basalts have relatively narrow ranges of Mg-numbers of 62.6–64.5, olivine compositions ($Fo_{85.8}$–$Fo_{86.3}$), and $(La/Sm)_{cn}$ ratios of 0.66–0.73, but rather variable CaO/Al_2O_3 ratios of 0.70–0.77 and Na_2O contents of 2.29–2.73 wt%. These Leg 158 basaltic whole-rock compositions have major-, trace-, and rare-earth–element characteristics similar to the glasses from this region. Fractional crystallization modeling using pseudoternary projections and liquid lines of descent calculations indicate that the Leg 158 basalts have probably undergone moderate pressure fractionation of olivine, then olivine + plagioclase at 4 to 6 kb, followed by rapid ascent from the upper mantle with very short crustal residence times. Multiple parental melt compositions are indicated by partial melting and fractional crystallization models. Maximum extents of partial melting in the upper mantle are estimated to be between ~11% and ~25% which is a larger variation than near the Kane Transform (MARK) area at ~10 to ~15%. The maximum extents of partial melting along the Mid-Atlantic Ridge show an overall decline from the Azores hotspot region (38°N) to the region south of the Hayes Transform (33°N), the TAG region (26°N), and Mid-Atlantic Ridge near the Kane Transform (MARK) area (23°N). Melt production and accumulation processes along the TAG segment, however, provide variability on the local scale.

INTRODUCTION AND OBJECTIVES

The slow-spreading Mid-Atlantic Ridge includes a ~750-km-long segment between the Atlantis (~30°N) and Kane (~24°N) major offset transforms. Seventeen non-transform (second- and third-order) discontinuities separate the Mid-Atlantic Ridge into 15- to 75-km-long segments offset by <1 to 30 km between the Atlantis and Kane transforms (Purdy et al., 1990; Sempéré et al., 1990; Smith and Cann, 1992). The active Trans-Atlantic Geotraverse (TAG) hydrothermal mound is located at 26°08′N, 44°49′W, midway along the 40-km-long segment defined by the second-order discontinuities at 25°55′N and 26°17′N (Rona et al., 1976; Purdy et al., 1990; Sempéré et al., 1990; Smith and Cann, 1992). The TAG segment exhibits no axial volcanic ridge within the rift valley, unlike the majority of the segments between the Atlantis and Kane transforms. This ridge segment, however, has numerous small volcanic seamounts (Smith and Cann, 1992).

The TAG hydrothermal mound is constructed on ~100,000-yr-old oceanic crust which, at the surface, is basaltic. The mound buildup rises 50 m above the seafloor at water depths of ~3650 m and is 200 m in diameter (Humphris et al., 1994). Massive pyrite and pyrite breccias comprise the uppermost layer of hydrothermal precipitates with pyrite-anhydrite breccias and pyrite-silica breccias occurring in the anhydrite zone beneath the massive pyrite zone. The stockwork zone consists of quartz-sulfide wallrock breccias and, in the deepest portions of the mound, quartz-chlorite breccias. Within the stockwork zone, slightly altered to highly altered basalts and metabasaltic clasts with high proportions of clay minerals are found. Silicified wallrock clasts are also found in the stockwork zone and are believed to represent totally altered basaltic clasts. Relatively unaltered basaltic basement beneath the hydrothermal precipitate buildup occurs at shallow levels around the edges of the mound but was not found at deep levels in the central portion of the mound (Humphris, Herzig, Miller, et al., 1996).

In this study, the influence of alteration on the basalts, hydrothermal clays, and metabasaltic clasts will be examined in order to compare the whole-rock geochemical changes between these basaltic rocks associated with hydrothermal alteration of the host mid-ocean ridge basalt (MORB) within the active TAG hydrothermal mound system. The whole-rock geochemistry of least-altered Leg 158 basalts will then be used to constrain the primary chemistry and the evolution of basaltic liquids along this portion of the Mid-Atlantic Ridge. The geochemical characteristics of the mantle source domain, the conditions of partial melting during magma generation in the oceanic upper mantle, and subsequent processes of melt pooling and fractional crystallization for the 26°N region of the Mid-Atlantic Ridge will be examined using major-, trace-, and rare-earth–element compositional variations and petrogenetic modeling. Mineral compositions also will provide constraints on the fractional crystallization processes that have affected these melts. Comparison of the Leg 158 basalts with the existing northern Mid-Atlantic Ridge data set will allow us to better constrain mantle source heterogeneities in the North Atlantic and magma generation processes along slow-spreading centers.

SAMPLE PREPARATION AND ANALYTICAL METHODS

The whole-rock samples were slabbed using a water-cooled diamond-blade saw, crushed by a high-strength iron carbide jaw crusher, and powdered in a tungsten carbide shatterbox. whole-rock powders were analyzed by inductively coupled plasma–atomic emission spectroscopy (ICP-AES) methods for major-, trace-, and rare-earth–element (REE) abundances on the Thermo Jarrell-Ash Atom Scan 25 spectrometer in the Department of Geosciences, University of Houston. For major-element (Si, Al, Fe, Mg, Ca) and trace-element (Na,

[1]Herzig, P.M., Humphris, S.E., Miller, D.J., and Zierenberg, R.A. (Eds.), 1998. *Proc. ODP, Sci. Results*, 158: College Station, TX (Ocean Drilling Program).

[2]Department of Geosciences, University of Houston, Houston, TX 77204-5503, U.S.A. sesmith@uh.edu

[3]Department of Geology and Geophysics, Woods Hole Oceanographic Institution, Woods Hole, MA 02543, U.S.A.

Prior Chapter Contents Next Chapter

P, K, Ti, V, Cr, Mn, Co, Ni, Cu, Zn, Sr, Zr, Ba) analyses, structural water was removed from sample powders by heating in a furnace at 1000°C for 30 minutes. Loss on ignition (LOI) was determined from the total weight change of the sample powder. Major and trace element analyses were performed on solutions in which the rock powder and $LiBO_2$ flux had been mixed, fused, and then dissolved in 1.5-N HNO_3. REE (La, Ce, Nd, Sm, Eu, Gd, Dy, Er, Yb), Sc, and Y analyses were conducted on solutions in which these elements had been isolated using standard cation exchange techniques. A detailed description of sample preparation and dilution methods is given in Smith (1994) and Meaux (1989). The measured elemental abundances in the major- and trace-element and REE solutions were calibrated against at least 5 USGS standards (AGV-1, BCR-1, BHVO-1, BIR-1, DNC-1, G-2, and W-2) and a $LiBO_2$ flux blank. Precisions and accuracies for these major-, trace-, and rare-earth–element ICP-AES methods are provided in Table 1. Mg-numbers ($100 \times Mg/[Mg+Fe^{2+}]$) are calculated using an assumed $Fe^{3+}/(Fe^{2+}+Fe^{3+})$ ratio of 0.10.

Polished thin sections were prepared for the Leg 158 basalts for petrographic examination and electron microprobe analysis of the primary mineral phases. The Cameca CAMEBAX SX-50 electron microprobe in the Department of Geology and Geophysics, Rice University, was utilized to analyze for olivine and plagioclase in basalts. For olivine analyses, an accelerating voltage of 15 keV, a beam current of 15 nA, and a 1- to 2-µm beam diameter were used. For plagioclase analyses, a beam current of 10 nA and a 10 µm beam diameter were used. The standards used for calibration checks were forsteritic olivine (Olivine 174.1), bytownite (Crystal Bay bytownite), and anorthite (Miyake anorthite). The "PAP" correction procedure was utilized for correction of oxides from microprobe analyses (Pouchou and Pichoir, 1985). Olivine compositions were very homogeneous and represent averaged core and rim analyses for 6 grains in each sample. Plagioclase compositions represent averaged core analyses for 4 grains in each sample. A complete listing of compositions and precision and accuracy values for the olivine and plagioclase standards is provided in Smith (1994).

Table 1. Precision and accuracy results for ICP-AES methods for major-, trace-, and rare-earth–element analyses at the University of Houston.

Oxide/Element	Precision (%)	Accuracy (%)
SiO_2	<2	<1
TiO_2	<3	<1
Al_2O_3	<3	<1
Fe_2O_3	<3	<1
MnO	<6	<1
MgO	<3	<1
CaO	<2	<1
Na_2O	<5	<7
K_2O	<11	<2
P_2O_5	<14	<4
Sc	<3	<2
V	<6	<3
Cr	<10	<19
Co	<24	<8
Ni	<15	<18
Cu	<11	<1
Zn	<11	<7
Sr	<6	<5
Y	<2	<5
Zr	<4	<9
Ba	<7	<8
La	<3	<7
Ce	<2	<2
Nd	<4	<6
Sm	<7	<4
Eu	<5	<1
Gd	<4	<1
Dy	<2	<2
Er	<4	<8
Yb	<4	<1

Notes: Precisions and accuracies for Si, Ti, Al, Fe, Mn, Mg, Ca, Na, K, P, Ba, Sr, Zr, V, Cr, and Ni were calculated from 10 separate fusions of BHVO-1 and 14 separate fusions of W-2. Precisions and accuracies for Co, Cu, and Zn were calculated from 8 separate fusions of W-2. Precisions and accuracies for Sc, Y, La, Ce, Nd, Sm, Eu, Gd, Dy, Er, and Yb were calculated from 14 separate fusions of BCR-1 and 14 separate fusions of W-2.

GEOCHEMISTRY AND PETROLOGY OF BASALTS, HYDROTHERMAL CLAYS, AND METABASALTIC CLASTS

The whole-rock samples have been divided into three groups: (1) basalts (Holes 957B and 957M), (2) hydrothermal clays (Hole 957B), and (3) metabasaltic clasts (Holes 957E, 957H, 957M, and 957P). Relatively unaltered basalt was first found on the southeast side of the TAG hydrothermal mound in the Kremlin area at a depth of ~20 meters below seafloor (mbsf) in Hole 957B (see Fig. 1 for hole locations), whereas on the western edge of the mound, basalt was first recovered at a depth of ~42 mbsf in Hole 957M. The presence of basalt was interpreted to represent basement below the TAG mound of hydrothermal precipitates (Humphris, Herzig, Miller, et al., 1996). Red hydrothermal clays also were recovered in Hole 957B and are believed to represent the hydrothermal alteration products of basalt (Humphris, Herzig, Miller, et al., 1996). The metabasaltic clasts in this study were recovered from the quartz-chlorite stockwork zone at a depth of ~106 mbsf in the central portion of the mound at Hole 957E (see Fig. 1) and at shallower levels at depths of ~29–50 mbsf along the outer perimeter of the mound in Holes 957H, 957M, and 957P (Humphris, Herzig, Miller, et al., 1996).

Basalts

The basalts are sparsely olivine phyric with intersertal textures. Olivine is the dominant phenocryst phase (<3 vol%) and occurs as euhedral grains. Plagioclase occurs as microlites in the groundmass. Fresh glass was not observed in any of the samples. Major-element analyses of olivine are listed in Table 2 and were performed on two samples from each of the Sections 158-957M-9R-1 (Samples 158-957M-9R-1, 67–71 cm, and 9R-1, 118-121 cm), 158-957M-10R-1 (Samples 158-957M-10R-1, 8–10 cm, and 117–120 cm), and 158-957M-10R-2 (Samples 158-957M-10R-2, 11–14 cm, and 35–38

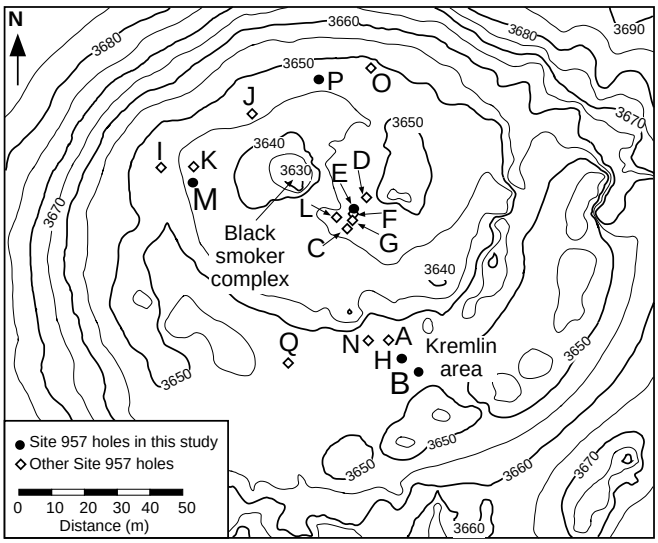

Figure 1. Topographic map of the TAG hydrothermal mound at 26°08′N, 44°49′W along the eastern flank of the Mid-Atlantic Ridge. Sample holes (Holes 957B, 957E, 957H, 957M, and 957P) discussed in this paper are shown with solid circles. The other holes (open diamonds) are shown for reference. Contour interval is 5 m. Map is after Humphris, Herzig, Miller, et al. (1996).

Table 2. Hole 957M olivine compositions.

Hole, core, section:	957M-9R-1		957M-9R-1		957M-10R-1	
Interval (cm):	67-71		118-121		8-10	
Oxide	Avg	±1 σ	Avg	±1 σ	Avg	±1 σ
SiO_2 (wt%)	39.24	0.15	39.60	0.22	39.60	0.27
FeO	13.33	0.23	13.02	0.26	13.40	0.20
NiO	0.32	0.06	0.35	0.06	0.23	0.07
MgO	46.15	0.30	46.06	0.21	46.34	0.24
CaO	0.28	0.03	0.30	0.02	0.31	0.02
Total	99.32	0.33	99.33	0.57	99.88	0.59
Fo (%)	86.0	0.3	86.3	0.2	86.1	0.1
Fa (%)	14.0	0.3	13.7	0.2	13.9	0.1

Hole, core, section:	957M-10R-01		957M-10R-02		957M-10R-02	
Interval (cm):	117-120		11-14		35-38	
Oxide	Avg	±1 σ	Avg	±1 σ	Avg	±1 σ
SiO_2 (wt%)	39.67	0.32	39.55	0.35	39.48	0.11
FeO	13.54	0.08	13.69	0.34	13.29	0.15
NiO	0.30	0.04	0.28	0.09	0.32	0.07
MgO	46.20	0.13	46.32	0.39	46.05	0.16
CaO	0.29	0.02	0.30	0.01	0.30	0.03
Total	99.99	0.36	100.13	0.53	99.43	0.29
Fo (%)	85.9	0.1	85.8	0.4	86.1	0.1
Fa (%)	14.1	0.1	14.2	0.4	13.9	0.1

Note: Avg = average.

cm). These olivines are unzoned and have a limited range of compositions of $Fo_{85.8}$-$Fo_{86.3}$ and 0.23–0.30 wt% NiO (Table 2). The Mg-numbers of liquids calculated to be in equilibrium with olivine phenocrysts in these basalts exhibit a range of 62.8 to 63.8 based on a K_D of 0.28 for Fe^{2+}-Mg exchange between olivine and a silicate liquid (Roeder and Emslie, 1970; Sigurdsson, 1981; Hess, 1992). Plagioclase microlites were analyzed in Samples 158-957M-9R-1, 67–71 cm, and 158-957M-10R-2, 11–14 cm, and exhibit average compositions of An_{61} and An_{64}, respectively. These microlites represent quench phases and would not be in equilibrium with the whole-rock composition or liquids calculated to be in equilibrium with coexisting olivine (Stakes et al., 1984).

Whole-rock major-, trace-, and rare-earth–element analyses of basalts are listed in Table 3 and consist of one sample from Hole 957B (Sample 158-957B-4R-1, 55–62 cm) and ten basalts from Hole 957M (Samples 158-957M-9R-1, 38–43 cm; 9R-1, 67–71 cm; 9R-1, 112–115 cm; 9R-1, 118–121 cm; 10R-1, 8–10 cm; 10R-1, 33–36 cm; 10R-1, 69–74 cm; 10R-1, 117–120 cm; 10R-2, 11–14 cm; 10R-2, 35–38 cm). In addition, the green and red altered rims from the Hole 957M basalts were analyzed separately from the interior of the samples. Samples 9R-1, 67–71 cm, and 10R-2, 11–14 cm, exhibited green alteration rims, and Samples 10R-1, 69–74 cm, and 10R-1, 117–120 cm, displayed red alteration rims. These four samples have the designation of "A" for the interior portion and "B" for the rim portions of the samples (see Table 3). The rim compositions will be considered separately from the interior samples and samples without rims. The green and red rims exhibit up to 70% total alteration. Smectite occurs as the product of hydrothermal alteration of the groundmass in the Hole 957M basalts (Sturz et al., Chap. 20, this volume), whereas smectite, talc, Fe-oxides, and/or Fe-oxyhydroxides represent the alteration products of the olivine phenocrysts. Pyrite also occurs as disseminated grains (up to 15%) in the red and green alteration rims but exhibits corroded grain edges in the green rims. The red rims are richer in Fe-oxides and Fe-oxyhydroxides compared to the green rims.

The Hole 957B basalt is slightly more primitive, with a Mg-number of 64.5 compared to the Hole 957M basalts that range from 54.9 to 64.2. The whole-rock Mg-numbers for Hole 957M basalts with olivine analyses are 60.8–63.5 which are comparable to that calculated for basaltic liquids in equilibrium with the olivine phenocrysts in these samples. Loss-on-ignition (LOI) values of 0.64%–2.04% indicate that these basalts are less altered compared to the green and red alteration rims in the Hole 957M basalts with LOI values up to 5.36%. As shown in Fig. 2, as LOI percentage increases, SiO_2, CaO, and Na_2O contents decrease and Al_2O_3, Fe_2O_3, MgO, Zn, Cr, and Zr abundances increase in the transition from the basaltic interior to the alteration rim compositions. The most extreme example of enrichment due to alteration by hydrothermal solutions is the elevated Zn concentrations in the alteration rims, from a baseline concentration in the least altered basalts of < 105 ppm to the rim concentration of 4316 ppm (Sample 158-957M-10R-2, 11–14B cm). The other green and red rim compositions also exhibit higher abundances of Zn (345 to 1572 ppm) than the interior compositions. Samples 158-957M-9R-1, 112–115 cm, 10R-2, 11–14A cm, and 10R-2, 35–38 cm, also contain Zn abundances of 201–357 ppm, which indicates a higher level of alteration compared to the relatively unaltered samples. X-ray diffraction analyses for Samples 158-957M-9R-1, 67–71B cm, with 1572 ppm Zn and 10R-1, 117–120B cm, with 961 ppm Zn were not conclusive in determining the Zn-enriched phase in these altered rims. Sturz et al. (Chap. 20, this volume) have suggested that the Zn enrichment may reside in smectite in the alteration rims.

The Hole 957B and 957M basalts from the TAG hydrothermal mound are N-type MORB with light-REE-depleted patterns at ~15 to 20× chondrite (Fig. 3A). N-type MORB are light REE-depleted basalts with $(La/Sm)_{cn}$ ratios of < 0.8, incompatible-element depleted (e.g., Cs, Rb, K, Ba, Sr, Zr, Nb), and have low $^{87}Sr/^{86}Sr$ values (Schilling, 1975; Bryan et al., 1976; Sun et al., 1979). The basalts, basaltic interiors, and altered rims exhibit light-REE-depleted patterns that are all virtually identical to each other.

Hydrothermal Clays

Samples 158-957B-4R-1, 25–27 cm, and 5B-1, 4–9 cm, are representative of the hydrothermal clay group, and their compositions are given in Table 4. With alteration of basalt to red chlorite (Sturz et al., Chap. 20, this volume), Fe-oxides, and Fe-oxyhydroxides, distinct decreases in SiO_2, CaO, Na_2O, and Sr contents in whole-rock compositions are observed (Table 4 and Fig. 2). Increases in Al_2O_3, Fe_2O_3, MgO, and Cr abundances are apparent relative to the basalt and the alteration rim compositions. Zn is only slightly higher than in the basalts. As shown in Fig. 3B, the Hole 957B hydrothermal clay samples are also light-REE-depleted and exhibit REE abundances

Table 3. Whole rock major-, trace-, and rare-earth-element compositions of Leg 158 basalts and alteration rims.

Hole, core, section:	957B-4R-1	957M-9R-1	957M-9R-1	957M-9R-1	957M-9R-1	957M-9R-1	957M-10R-1	957M-10R-1	957M-10R-1	957M-10R-1	957M-10R-1	957M-10R-1	957M-10R-2	957M-10R-2	957M-10R-2
Interval (cm):	55-62	38-43	67-71A	67-71B	112-115	118-121	8-10	33-36	69-74A	69-74B	117-120A	117-120B	11-14A	11-14B	35-38
Rock type	Basalt	Basalt	Basalt interior	Altered green rim	Basalt	Basalt	Basalt	Basalt	Basalt (interior)	Altered red rim	Basalt (interior)	Altered red rim	Basalt (interior)	Altered green rim	Basalt
Oxide															
SiO_2 (wt%)	49.97	50.38	49.79	47.77	49.71	50.13	50.60	49.74	49.90	48.29	49.40	48.68	49.77	42.77	50.08
TiO_2	1.61	1.59	1.59	1.75	1.60	1.60	1.53	1.60	1.66	1.70	1.59	1.66	1.66	1.92	1.66
Al_2O_3	15.05	15.31	14.73	16.11	15.12	14.68	15.19	14.96	14.81	15.41	14.40	15.11	15.02	17.78	15.34
Fe_2O_3	11.27	10.96	11.20	13.25	10.98	11.17	10.91	10.89	11.01	12.75	11.09	12.19	11.17	19.24	11.53
MnO	0.17	0.15	0.18	0.11	0.17	0.19	0.17	0.19	0.19	0.15	0.17	0.16	0.15	0.09	0.14
MgO	9.34	8.72	8.84	8.62	8.36	8.84	8.57	8.72	8.98	9.88	8.45	7.83	8.49	10.63	8.14
CaO	11.03	10.69	10.78	8.59	10.48	11.10	10.60	11.01	10.37	8.90	11.04	10.80	10.46	4.62	10.39
Na_2O	2.29	2.59	2.55	2.62	2.73	2.66	2.72	2.73	2.64	2.44	2.73	2.95	2.77	2.23	2.78
K_2O	0.08	0.09	0.13	0.11	0.13	0.17	0.10	0.16	0.30	0.48	0.13	0.14	0.08	0.06	0.12
P_2O_5	0.16	0.15	0.16	0.17	0.16	0.16	0.15	0.16	0.16	0.15	0.15	0.16	0.16	0.18	0.16
Total	100.96	100.64	99.95	99.10	99.44	100.70	100.53	100.16	100.03	100.15	99.15	99.68	99.73	99.53	100.33
LOI (%)	1.89	1.69	1.76	2.56	1.29	1.02	1.00	0.80	2.04	3.67	0.64	1.25	1.96	5.36	1.62
$100 \times (Mg/[Mg+Fe^{2+}])$	64.5	63.6	63.5	58.9	62.6	63.5	63.4	63.8	64.2	63.0	62.6	58.6	62.6	54.9	60.8
CaO/Al_2O_3	0.73	0.70	0.73	0.53	0.69	0.76	0.70	0.74	0.70	0.58	0.77	0.71	0.70	0.26	0.68
Element															
Sc (ppm)	39	39	39	41	40	38	38	38	38.8	39.7	39	40	40	n.d.	40
V	302	312	312	331	301	306	300	324	316.6	301.2	294	311	314	380	305
Cr	294	308	316	343	319	314	345	317	316.7	357.5	327	346	331	458	345
Co	98	43	48	61	53	49	57	68	50.8	48.0	58	62	56	55	55
Ni	121	119	127	128	131	120	118	114	118.5	189.9	129	116	129	127	158
Cu	84	78	72	87	80	70	75	79	71.7	71.4	78	75	80	108	78
Zn	78	99	103	1572	297	90	83	88	92.3	345.4	95	961	201	4316	357
Sr	117	114	112	117	121	118	115	124	136.7	135.6	123	127	118	91	117
Y	38	39	39	40	39	38	38	37	39.1	38.2	39	39	39	n.d.	39
Zr	102	101	100	110	102	102	100	109	107.5	109.7	101	107	106	125	107
Ba	12	10	12	11	12	14	12	16	22.4	27.2	14	15	10	10	10
La	3.5	3.8	3.8	4.1	3.9	3.7	3.7	3.3	3.9	3.8	3.9	4.0	4.0	n.d.	3.8
Ce	12.0	12.1	11.9	12.9	12.1	11.9	12.0	11.7	12.3	12.2	12.1	12.7	12.4	n.d.	12.3
Nd	10.8	10.8	11.1	11.7	10.7	10.8	10.7	10.5	11.4	11.1	11.0	11.4	11.3	n.d.	11.1
Sm	3.3	3.3	3.4	3.5	3.4	3.2	3.4	3.1	3.3	3.3	3.4	3.6	3.6	n.d.	3.5
Eu	1.32	1.38	1.34	1.46	1.37	1.31	1.28	1.27	1.37	1.30	1.34	1.39	1.38	n.d.	1.30
Gd	4.9	4.9	4.9	5.1	5.0	4.9	4.8	4.8	5.0	4.9	5.0	5.1	5.1	n.d.	5.0
Dy	5.9	6.4	6.3	6.5	6.4	6.2	6.3	5.8	6.3	6.3	6.4	6.5	6.5	n.d.	6.4
Er	3.8	4.2	4.1	4.4	4.2	4.1	4.1	3.7	4.2	4.1	4.1	4.2	4.2	n.d.	4.2
Yb	3.5	3.6	3.7	3.8	3.7	3.5	3.6	3.5	3.7	3.7	3.7	3.7	3.7	n.d.	3.7
$(La/Sm)_{cn}$	0.66	0.72	0.69	0.73	0.72	0.72	0.68	0.67	0.73	0.73	0.72	0.70	0.70	n.d.	0.67
$(La/Yb)_{cn}$	0.68	0.73	0.71	0.74	0.73	0.73	0.72	0.66	0.73	0.71	0.73	0.75	0.75	n.d.	0.70

Notes: n.d. = not determined. Chondrite normalization is from Anders and Grevesse (1989). Eu/Eu* is calculated as $Eu_{cn}/(Sm_{cn} \times Gd_{cn})^{0.5}$ from McLennan (1989). Sr/Sr* is similarly calculated as $St_{cn}/(Ce_{cn} \times Nd_{cn})^{0.5}$, Zr/Zr* as $Zr_{cn}/(Nd_{cn} \times Sm_{cn})^{0.5}$, and Ti/Ti* as $Ti_{cn}/(Gd_{cn} \times Dy_{cn})^{0.5}$.

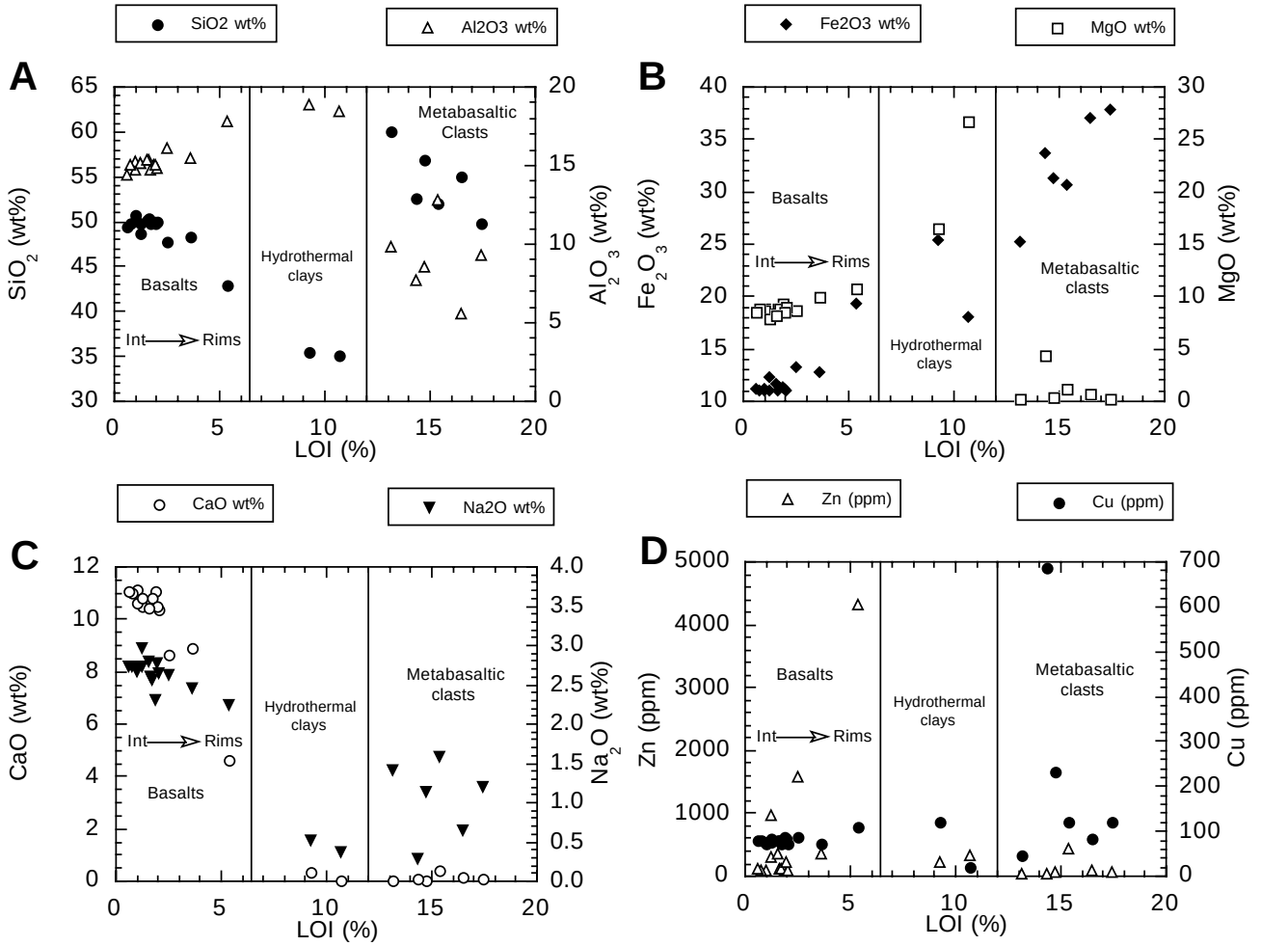

Figure 2. **A.** LOI (%) vs. SiO_2 (wt%) and Al_2O_3 (wt%). **B.** LOI (%) vs. Fe_2O_3 (wt%) and MgO (wt%). **C.** LOI (%) vs. CaO and Na_2O (wt%). **D.** LOI (%) vs. Zn (ppm) and Cu (ppm).

very similar to the Hole 957B and 957M basalts, basaltic interiors, and altered rims. However, the clays have prominent Eu/Eu* anomalies (0.75–1.20) unlike the Hole 957B and 957M basalts which have only slight Eu/Eu* anomalies (0.98–1.05).

Metabasaltic Clasts

Metabasaltic clasts from the quartz-chlorite stockwork zone of the TAG hydrothermal mound consist of quartz, gray chlorite, and disseminated sulfides. Within the clasts, relict igneous textures are generally preserved and indicate textures similar to the basalts from Holes 957B and 957M. Gray chlorite represents the alteration of the basalt fragments, whereas quartz and pyrite may occur as disseminated grains or as vein filling. Pyrite abundances ranges up to 20 vol%. Quartz may also occur as a replacement for plagioclase microlites. The altered basaltic clasts from the stockwork zone, however, contain low concentrations of MnO, CaO, MgO, and Na_2O, whereas SiO_2 and Fe_2O_3 contents are elevated relative to the basalts (Table 5 and Fig. 2). Cr abundances are variable for the clasts. Cu concentrations also are variable, but the metabasaltic clasts have chalcopyrite present. Zn, Sr, Zr, and Y contents are generally lower in the metabasaltic clasts compared to the basalts (Fig. 2).

The REE abundances are significantly lower for the metabasaltic clasts compared to the basalts. The REE patterns for these metabasaltic clasts are unlike the light-REE-depleted patterns of the basalts and hydrothermal clays (Fig. 3C). The REE patterns for all of the metabasaltic clasts have $(La/Sm)_{cn}$ ratios of > 0.90 compared to the basalts with ratios of < 0.75. The Section 158-957E-15R-1, 158-957E-16R-1, 158–957E-17R-1, and 158-957P-11R-1 metabasaltic clasts exhibit the largest negative Eu/Eu* anomalies (0.33–0.72) of the entire sample suite.

Comparison of Basalts, Hydrothermal Clays and Metabasaltic Clasts

The changes in whole-rock composition from basalt to smectite (Hole 957M alteration rims) or chlorite (Hole 957B clays and Holes 957E, 957H, 957M, and 957P clasts) by hydrothermally-derived fluids probably reflect variations of fluid compositions in the TAG hydrothermal system. In general, Fe_2O_3 contents increased and CaO contents decreased as alteration progressed. SiO_2 and MgO exhibit more complicated trends for the metabasaltic clasts compared to the basalts and hydrothermal clays because of the addition of quartz and pyrite to the whole-rock composition, such that SiO_2, Fe_2O_3, and MgO contents should be comparable to the hydrothermal clays if the quartz and pyrite abundances are subtracted (see Table 1, Sturz et al., Chap. 20, this volume). The sequence of Section 158-957M-9R-1 green rims, 10R-1 red rims, and 10R-2 green rims indicates the variability and vertical zonation of fluid compositions. Samples with red alteration rims contain high abundances of Fe-oxides and Fe-oxyhy-

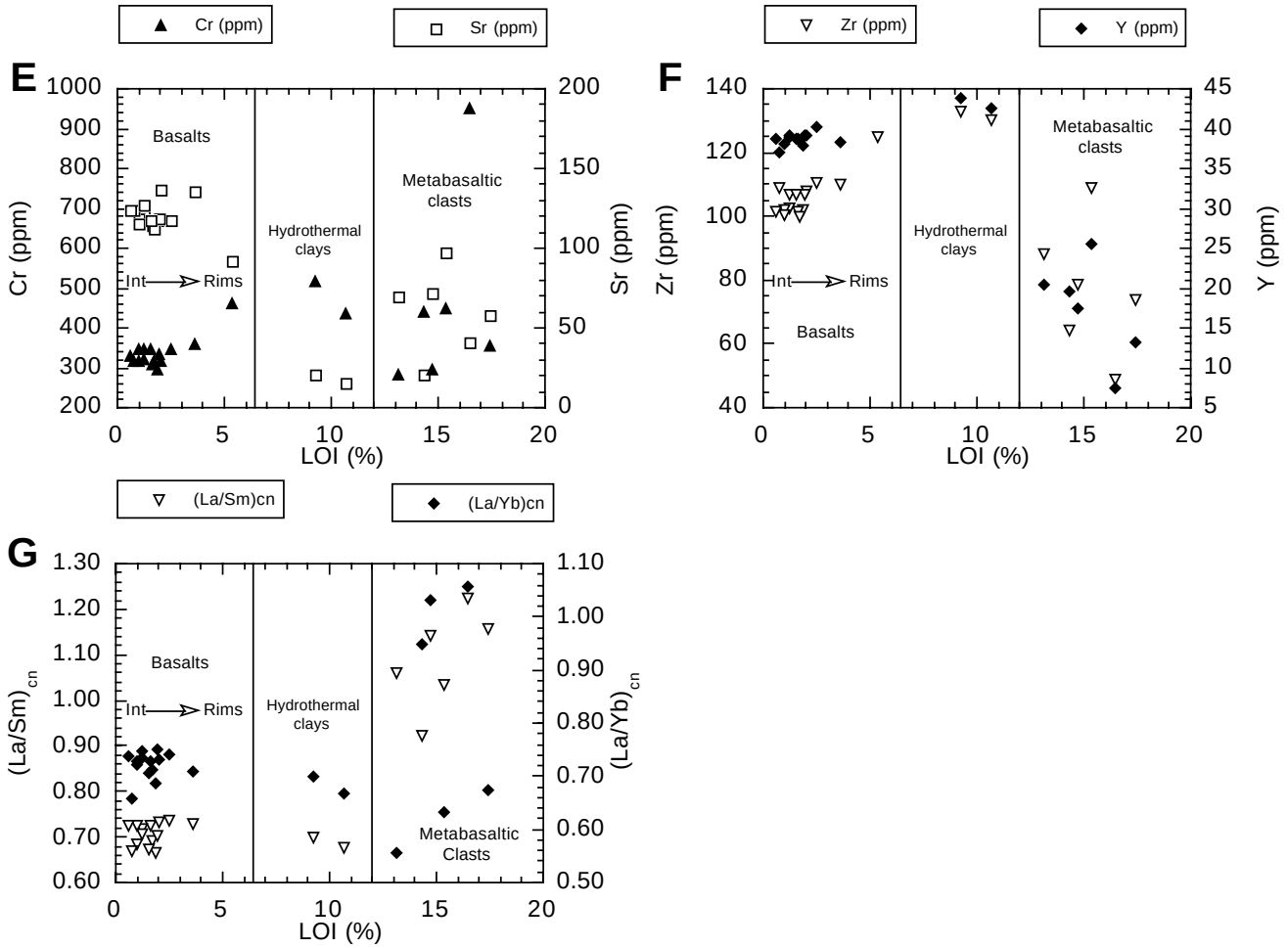

Figure 2 (continued). **E.** LOI (%) vs. Cr (ppm) and Sr (ppm). **F.** LOI (%) vs. Zr (ppm) and Y (ppm). **G.** LOI (%) vs. $(La/Sm)_{cn}$ and $(La/Yb)_{cn}$ variation diagrams. All data from this study are shown for the basalts, basaltic interiors (Int) and altered rims (Rim), hydrothermal clays, and metabasaltic clasts.

droxides in the rims compared to the samples with green alteration rims. Both Hole 957M red and green rims exhibit Zn enrichments of 345–961 ppm and 1572–4316 ppm, respectively, indicating that both types of hydrothermal fluids that affected the basalts on the western side of the TAG mound were, in general, more Zn-enriched than the fluids in the southeastern portion of the mound from compositions of Hole 957B hydrothermal clays with 207–330 ppm Zn.

REE abundances in the basalts, altered rims, and hydrothermal clays exhibit light-REE-depleted patterns that are all virtually identical to each other, suggesting that the REEs have not been mobilized by the Zn-enriched solutions that have affected some of the samples. The REE patterns of the metabasaltic clasts, however, show evidence of mobilization of Eu with strong negative anomalies, unlike the basalts and hydrothermal clays by hydrothermal fluids in the active TAG hydrothermal system.

COMPARISON OF THE GEOCHEMISTRY OF LEG 158 BASALTS WITH MORB FROM 20°N TO 40°N, MID-ATLANTIC RIDGE

In order to evaluate the evolution of magmatic liquids through partial melting and fractional crystallization, basalts with high LOI values, low CaO/Al_2O_3 ratios, and elevated Zn contents that reflect alteration effects have been excluded from our modeling. All of the Hole 957M alteration rim samples, therefore, are excluded as well as Samples 158-957M-9R-1, 112–115 cm, 158-957M-10R-2, 11–14A cm, and 158-957M-10R-2, 35–38 cm, which have Zn concentrations greater than 200 ppm. Additionally, the hydrothermal clay and metabasaltic clast samples will not be considered in this discussion. Below we compare the major-, trace-, and rare-earth–element geochemical characteristics of the Leg 158 basalts with other basalts from the TAG segment of the Mid-Atlantic Ridge, on-axis Mid-Atlantic Ridge basalts, on-axis Leg 46 and 106/109 basalts, and off-axis Leg 49 and 82 basalts.

Major-Element Geochemistry

The Leg 158 whole rocks (26.13°N) exhibit Mg-numbers between 62.6 and 64.5, CaO/Al_2O_3 ratios of 0.70–0.77, and Na_2O contents of 2.29–2.73 wt%. Leg 158 basalt compositions lie within the ranges of glasses recovered in the TAG region of the Mid-Atlantic Ridge from 26.04°N to 26.25°N (Meyer and Bryan, 1996) with Mg-numbers of 57.1–71.0 and CaO/Al_2O_3 ratios of 0.70–0.80, and Na_2O contents of 1.82–2.95 wt% (Fig. 4). Leg 46 and 106/109 glasses and whole rocks from the Kane Transform region (~23°N), however, exhibit slightly more evolved compositions compared to the TAG region with Mg-numbers of 53.1–67.3, CaO/Al_2O_3 ratios of 0.66–0.78, and Na_2O contents of 2.43–3.14 wt% (Dungan et al., 1978; Sato et al., 1979; Humphris et al., 1990).

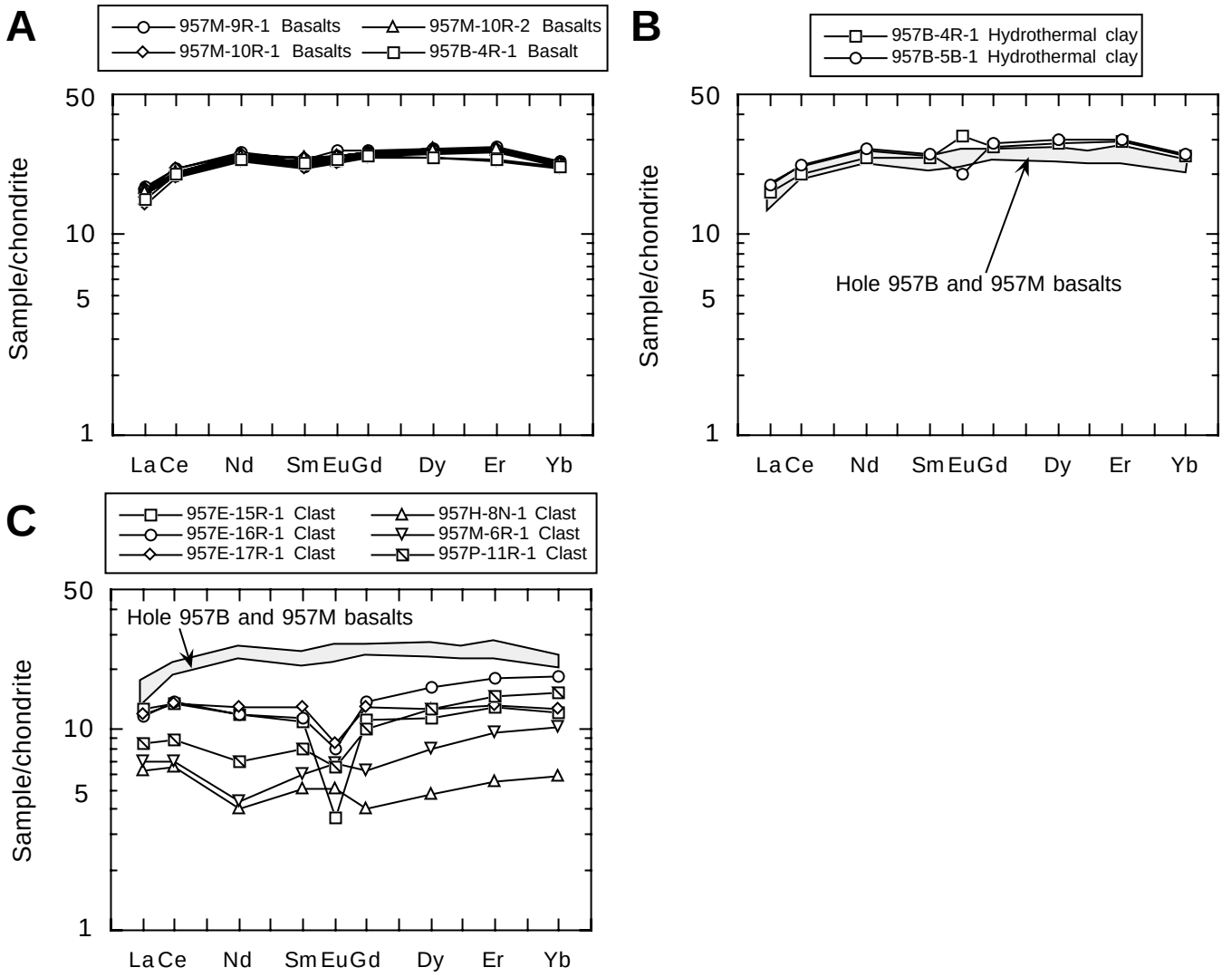

Figure 3. Rare-earth–element variation diagrams. **A.** Hole 957B and 957M basalts, basaltic interiors, and green/red altered rims. **B.** Hole 957B hydrothermal clays. **C.** Hole 957E, 957H, 957M, and 957P metabasaltic clasts. Also displayed in (B) and (C) is the field of the Hole 957B and 957M basalts. Chondrite normalization values from Anders and Grevesse (1989).

Trace- and Rare-Earth–Element Geochemistry

The oceanic mantle is currently viewed as chemically heterogeneous on centimeter to kilometer scales with reference to trace elements, REEs, and isotopic systems. Multiple enriched to depleted source domains have been proposed for MORB and ocean island basalts. They include depleted mantle, primordial mantle, recycled oceanic lithosphere, and subcontinental upper mantle (Sun et al., 1979; Cohen and O'Nions, 1982; White and Hofmann, 1982; Zindler et al., 1982; Hamelin et al., 1984; Allègre and Turcotte, 1986; Ito et al., 1987; Prinzhofer et al., 1989; Sun and McDonough, 1989). The primitive mantle is thought to have been enriched in REEs at 2–3× chondrite unlike the upper mantle which is light-REE-depleted with ~1.5× chondrite for the light REEs (Loubet et al., 1975; McDonough and Frey, 1989; Sun and McDonough, 1989). Typical depleted oceanic upper mantle alone will generate basaltic liquids that are N-type MORB from a reservoir that has undergone a long term (>1 Ga) depletion of Nd relative to Sm and Rb (DePaolo and Wasserburg, 1976a, 1976b).

Only N-type MORB is found south of the Hayes Transform (~33°40′N), as shown in Figure 5. The Leg 158 basalts reported on here and the basaltic glasses from TAG (Meyer and Bryan, 1996) exhibit $(La/Sm)_{cn}$ ratios of 0.66–0.73 and 0.39–0.71, respectively, typical of N-type MORB. Figure 5 shows that N-type MORB is erupted exclusively along the Mid-Atlantic Ridge from 22°N, just south of the Kane Transform, to 33°40'N, just south of the Hayes Transform. North of the Hayes Transform, basalts show increasing enrichments in $(La/Sm)_{cn}$ ratios as the Azores region is approached. Such variation in basalt geochemistry along with Sr-Nd-Pb isotopic evidence indicates depleted upper mantle south of the Hayes Transform and both depleted and enriched upper mantle north of the Hayes Transform (Schilling, 1975; White and Schilling, 1978; Schilling et al., 1983; Hamelin et al., 1984; Bougault et al., 1985; Drake et al., 1985; Dupré et al., 1985; Hertogen et al., 1985; Jenner et al., 1985; Rideout and Schilling, 1985; Weaver et al., 1985; Smith, 1994). Spidergrams (Fig. 6) of the Leg 158 basalts correspond to the upper end of the field of Mid-Atlantic Ridge glass patterns from the TAG region (26.04°N–26.25°N; Meyer and Bryan, 1996). The TAG glasses show large ranges of Sr/Sr* anomalies (0.47–1.37) and Zr/Zr* anomalies (0.82–1.40). The Hole 957B and 957M basalts exhibit negative Sr/Sr* anomalies of 0.65–0.78 and positive Zr/Zr* anomalies of 1.07–1.25, similar to the most enriched TAG glasses (Fig. 6). The negative Na

Table 4. Whole rock major-, trace-, and rare-earth-element compositions of Leg 158 hydrothermal clays.

Hole, core, section:	957B-4R-1	957B-5B-1
Interval (cm):	25-27	4-9
Oxide		
SiO_2 (wt%)	35.13	35.41
TiO_2	2.07	2.02
Al_2O_3	18.46	18.87
Fe_2O_3	17.92	25.29
MnO	0.07	0.06
MgO	26.61	16.41
CaO	0.00	0.35
Na_2O	0.35	0.51
K_2O	0.04	0.03
P_2O_5	0.07	0.04
Total	100.71	98.99
LOI (%)	10.70	9.26
Element		
Sc (ppm)	44	46
V	322	376
Cr	432	514
Co	54	64
Ni	146	151
Cu	19	121
Zn	330	207
Sr	15	20
Y	42	44
Zr	130	133
Ba	10	10
La	3.9	4.2
Ce	12.1	13.3
Nd	10.9	12.1
Sm	3.6	3.7
Eu	1.73	1.13
Gd	5.4	5.6
Dy	6.9	7.2
Er	4.6	4.7
Yb	4.0	4.1
$(La/Sm)_{cn}$	0.67	0.70
$(La/Yb)_{cn}$	0.67	0.70

anomalies for the basalts shown in Figure 6 is an artifact of chondrite normalization value of Na, which is depleted relative to the trace- and rare-earth–element abundances. The implications for these anomalies will be discussed in the trace-element modeling section.

FRACTIONAL CRYSTALLIZATION AND PARTIAL MELTING MODELING RESULTS FOR LEG 158 BASALTS

Major-Element Modeling

Major-element fractional crystallization modeling is presented with estimations of parental melt compositions, pressure of fractionation, and extent of fractionation. Major-element modeling involving the extent and initial depth of partial melting in the spinel lherzolite facies is also examined. Basaltic glass and whole-rock compositions will be used to calculate liquid lines of descent and to estimate the extent and depth of partial melting required to generate the calculated parental liquids of these samples (Klein and Langmuir, 1987, 1989; Weaver and Langmuir, 1990; Niu and Batiza, 1991).

Olivine-Clinopyroxene-Quartz-Plagioclase Pseudoternary Projections

Basaltic glass and whole-rock compositions can be shown on pseudoternary projections of olivine-clinopyroxene-quartz (+plagioclase) in order to demonstrate the relationships between the end-member mineral phases as related to temperature and pressure. Pseudoinvariant points for olivine, plagioclase, clinopyroxene, and low-Ca pyroxene crystallization were determined for a range of pressures from 0.001 to 6 kb for glass sample TAG75-1B-21, from Meyer and Bryan (1996), as shown in Figure 7. These pseudoinvariant points are based on the projection schemes of Grove et al. (1992). The

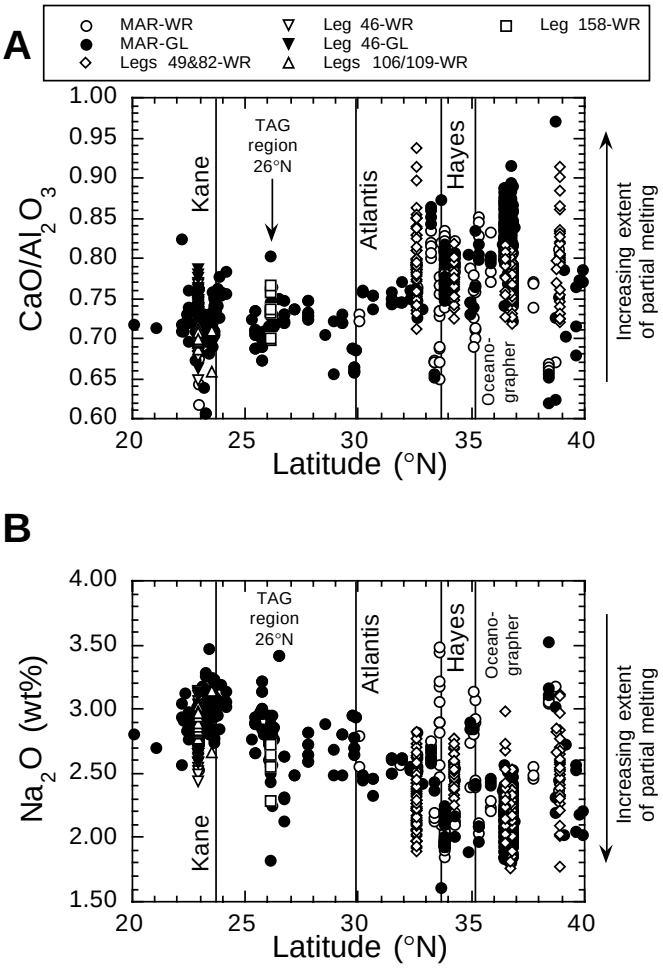

Figure 4. Latitude (°N) vs. CaO/Al_2O_3 (**A**) and latitude (°N) vs. Na_2O (wt%) (**B**) variation diagrams for Mid-Atlantic Ridge basalts from 20°N to 40°N. The locations of the Kane, Atlantis, Hayes, and Oceanographer major offset transforms are displayed. The "zero-age" Mid-Atlantic Ridge basalts shown in these figures represent samples from either dredge or dive collections and include glass (GL) and whole-rock (WR) compositions. The locations of the off-axis Leg 49 and 82 DSDP basalts have been projected back to the Mid-Atlantic Ridge along single flow lines. Data are from: Shibata and Fox (1975), Langmuir et al. (1977), Dungan et al. (1978), Sato et al. (1979), Tarney et al. (1979), O'Donnell and Presnall (1980), Sigurdsson (1981), Schilling et al. (1983), Dmitriev et al. (1985), Drake et al. (1985), Weaver et al. (1985), Melson and O'Hearn (1986), Humphris et al. (1990), Dmitriev et al. (1991), Bryan et al. (1994), Smith (1994), and Meyer and Bryan (1996).

boundary curves for crystallization of olivine, plagioclase, and clinopyroxene at these pressures are based on calculated liquid lines of descent for the presumed parental basalt composition. Meyer and Bryan (1996) suggested that TAG liquids may have been fractionated at pressures between 2 and 6 kb but concluded that the majority of the glasses from the TAG region appear multiply saturated near the 6 kb boundary indicating moderate pressures of fractionation. The Hole 957B and 957M whole rocks also plot along the 4 to 6 kb boundaries (Fig. 7) indicating multiple phase saturation at moderate pressures.

Parental Melts and Calculated Liquid Lines of Descent

In order to analyze further the physical conditions and extents of fractionation, low- to high-pressure fractionation models for each glass and whole-rock population have been determined relative to calculated parental melts. Parental liquid compositions have been de-

Table 5. Whole rock major-, trace-, and rare-earth–element compositions of Leg 158 metabasaltic clasts.

Hole, core, section, Interval (cm):	957E- 15R-1, 20-27	957E- 16R-1, 9-13	957E- 17R-1, 41-41	957H- 8N-1, 83-90	957M- 6R-1, 32-34	957P- 11R-1, 53-55
Oxide						
SiO_2 (wt%)	56.80	52.07	52.62	54.88	49.82	60.07
TiO_2	1.14	1.59	0.95	0.60	1.07	1.27
Al_2O_3	8.51	12.76	7.70	5.55	9.29	9.83
Fe_2O_3	31.21	30.63	33.64	36.95	37.83	25.24
MnO	0.00	0.01	0.02	0.00	0.00	0.00
MgO	0.40	1.20	4.26	0.65	0.14	0.15
CaO	0.00	0.36	0.07	0.15	0.07	0.02
Na_2O	1.14	1.58	0.29	0.65	1.18	1.41
K_2O	0.21	0.29	0.03	0.09	0.14	0.22
P_2O_5	0.03	0.03	0.02	0.02	0.01	0.01
Total	99.44	100.50	99.61	99.54	99.55	98.22
LOI (%)	14.75	15.40	14.35	16.48	17.44	13.14
Element						
Sc (ppm)	17	28	17	10	20	22
V	206	275	173	131	204	213
Cr	292	449	439	950	354	281
Co	488	1227	689	738	410	603
Ni	58	80	226	1679	53	57
Cu	232	119	684	81	120	44
Zn	43	424	30	92	60	31
Sr	72	97	21	40	57	69
Y	17	26	20	7	13	20
Zr	79	108	64	49	74	88
Ba	26.5	27	10	16	32	25
La	3.0	2.8	2.8	1.5	1.6	2.0
Ce	8.1	8.3	8.2	3.9	4.2	5.4
Nd	5.4	5.3	5.8	1.8	2.0	3.1
Sm	1.6	1.7	1.9	0.8	0.9	1.2
Eu	0.20	0.45	0.48	0.29	0.38	0.36
Gd	2.2	2.7	2.6	0.8	1.2	2.0
Dy	2.8	4.0	3.1	1.2	2.0	3.1
Er	2.1	2.9	2.1	0.9	1.6	2.3
Yb	2.0	3.0	2.1	1.0	1.7	2.5
$(La/Sm)_{cn}$	1.14	1.03	0.92	1.22	1.15	1.06
$(La/Yb)_{cn}$	1.03	0.63	0.95	1.05	0.67	0.56

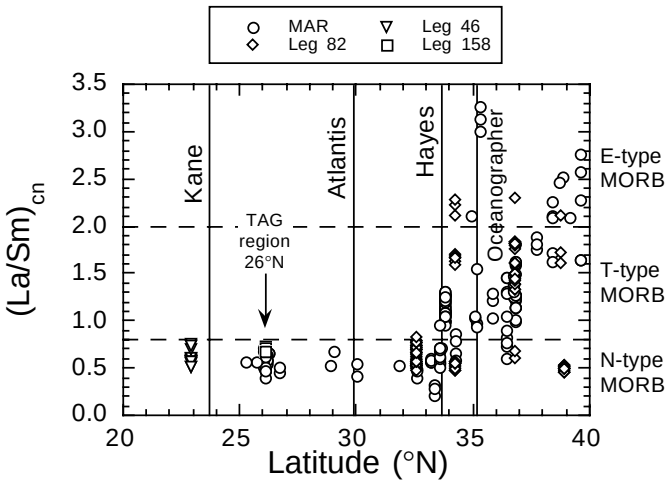

Figure 5. Latitude (°N) vs. $(La/Sm)_{cn}$ variation diagram for Mid-Atlantic Ridge basalts from 20°N to 40°N. The locations of the Kane, Atlantis, Hayes, and Oceanographer major offset transforms are displayed. Data are from Schilling (1975), Langmuir et al. (1977), Dungan et al. (1978), White and Bryan (1977), Schilling et al. (1983), Brannon (1985), Hertogen et al. (1985), Rideout and Schilling (1985), Frey et al. (1993), Smith (1994), and Meyer and Bryan (1996).

termined by back calculation involving olivine and plagioclase addition to the known samples such that liquids with Mg-numbers of 71–72 are obtained. These parental melts would then be in equilibrium in a mantle assemblage with ~Fo_{90} olivine. Fo_{90} is considered a minimum value for the TAG region mantle olivine. The crystallization program, "PETROLOG v. 1.00," by Danyushevsky (1991) was used

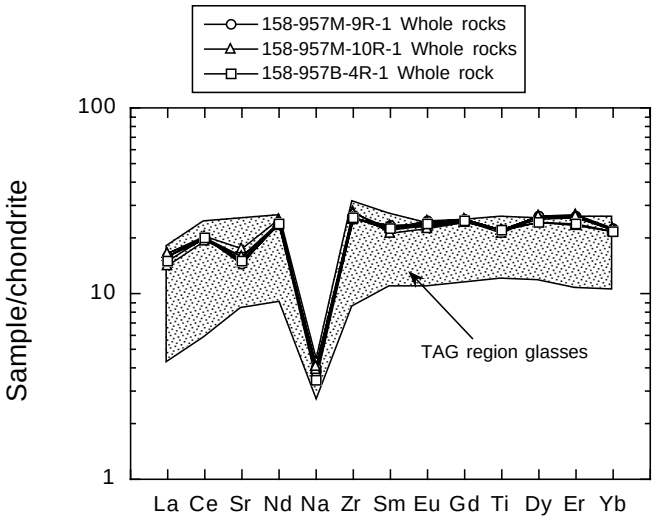

Figure 6. Spidergrams for the Section 158-957B-4R-1, 158-957M-9R-1, and 158-957M-10R-1 basalts utilized in fractional crystallization and partial melting modeling. The field for basaltic glass compositions from the TAG region (rift valley and eastern wall) of the Mid-Atlantic Ridge from Meyer and Bryan (1996) is shown for comparison. Element incompatibility order from Pearce and Parkinson (1993). Chondrite normalization values from Anders and Grevesse (1989).

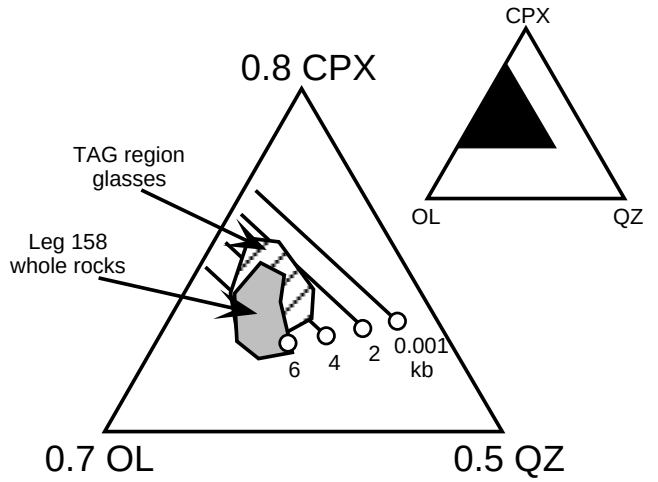

Figure 7. Pseudoternary olivine (OL)-clinopyroxene (CPX)-quartz (QZ) projections of Leg 158 whole rocks (this study) and TAG region glasses (Meyer and Bryan, 1996) using the projection scheme from Grove et al. (1992). Open circles are calculated boundaries (points) for TAG75-01B-21 (glass from Meyer and Bryan, 1996) at pressures of 0.001, 2, 4, and 6 kb where olivine, plagioclase, augite, low-Ca pyroxene, and melt are in equilibrium. The line boundaries are taken from calculated liquid lines of descent for the same glasses used in the boundary point calculations and represent where olivine, plagioclase, augite, and melt are in equilibrium.

to back calculate to parental melt compositions using mineral assemblages of olivine + plagioclase and olivine only. A MgO content of 9.0 wt% was chosen for initiation of plagioclase fractionation based on the calculation of liquid lines of descent. The basaltic liquid lines of descent were calculated using the FORTRAN program "BASALT" from Weaver and Langmuir (1990), which determines mineral/melt equilibria over a range of pressures. Calculated liquid lines of descent from an actual sample and from its predicted parental melt both coincide using the algorithm of Weaver and Langmuir (1990);

therefore a back calculation to estimate the parental melt composition using the algorithm of Danyushevsky (1991) does not alter the fractional crystallization path of that sample.

In order to show the range in parental melt compositions, glass data from Meyer and Bryan (1996) are used with the Leg 158 whole-rock data to bracket the limits of variability in this region. Of the four primitive samples modeled, three are represented by glass compositions (TAG75-01B-21, TAG77-07-10, and AII-129-5, 1–3; Meyer and Bryan, 1996), and one is a whole-rock composition (Sample 158-957B-4R-1, 55–62 cm). The model parental compositions, LLD-TAG-A, LLD-TAG-B, LLD-TAG-C, and LLD-TAG-D, have been determined by back calculation involving olivine or olivine and plagioclase addition to the samples noted above and are listed in Table 6.

From olivine-clinopyroxene-quartz (+plagioclase) pseudoternary projections (Fig. 7) and Meyer and Bryan (1996), the pressure of fractionation for the Leg 158 probably ranges from 4 to 6 kb. Results of the fractional crystallization modeling at 6 kb are given in Table 7 for representative Samples 158-957B-4R-1, 55–62 cm, and 158-957M-10R-1, 8–10 cm. The fractional crystallization calculations suggest that Sample 158-957M-10R-1, 8–10 cm, experienced a total of 29% crystallization of olivine then olivine + plagioclase using LLD-TAG-A. Sample 158-957B-4R-1, 55–62 cm, is predicted through modeling to have undergone 15% fractionation of olivine using LLD-TAG-D. Calculated liquid lines of descent for the model parents are shown in Figure 8 at pressures of 1 atm to 6 kb. TAG region glass compositions from 26.04°N to 26.25°N (Meyer and Bryan, 1996) are also displayed for comparison with the Leg 158 basalts. As shown in Figures 8A and 8B, the Section 158-957M-9R-1 and 158-957M-10R-1 basalts suggest olivine, then olivine + plagioclase fractionation, whereas the LLD-TAG-C model predicts olivine only fractionation for Sample 158-957B-4R-1, 55–62 cm.

From the pseudoternary projections and liquid lines of descent calculations, the Leg 158 whole rocks and TAG region glasses appear to have undergone rapid ascent from 6 kb (18 km) without long residence times in crustal level magma chambers beneath the TAG ridge segment, as suggested by Meyer and Bryan (1996). Multiple parental melts produced along the TAG segment are required to account for the compositional variability of the TAG region glasses and Leg 158 basalts. The presence of a large magma chamber in the crust beneath the TAG segment that controls melt pooling, magma mixing, and low-pressure fractionation of ascending melt packages is not supported by the basalt geochemical characteristics. The presence of numerous small seamounts along this ridge segment (Smith and Cann, 1992) would indicate that small, isolated magma chambers or lenses instead may be present in the crust.

Table 6. Calculated parental liquid starting compositions used in fractional crystallization modeling.

Model composition	LLD-TAG-A	LLD-TAG-B	LLD-TAG-C	LLD-TAG-D
SiO_2 (wt%)	49.49	49.14	48.83	49.79
TiO_2	1.00	1.10	1.38	0.80
$A_{l2}O_3$	16.68	14.19	12.90	14.99
FeO*	8.03	9.29	10.34	8.39
MgO	11.68	13.86	15.13	12.31
CaO	10.64	10.14	9.45	12.01
Na_2O	2.50	2.28	1.96	1.70
$(Mg/[Mg + \Sigma Fe]) \times 100$	72.2	72.6	72.3	72.3
CaO/Al_2O_3	0.64	0.71	0.73	0.80
Equilibrium olivine	$Fo_{90.7}$	$Fo_{90.7}$	$Fo_{90.6}$	$Fo_{90.7}$
Olivine addition (wt%)	11	12	15	7
Plagioclase addition (wt%)	14	0	0	0
Sample number	TAG75-01B-21	TAG77-07-10	158-957B-4R-1 (55-62)	AII-129-5, 01-03
Sample type	Glass	Glass	Whole-rock	Glass

Notes: Compositions shown above are normalized to 100 wt% and represent back calculated parental fractional crystallization liquid compositions for the samples indicated at the bottom of the table. The actual glass compositions for TAG75-01B-21, TAG77-07-10, and AII-129-5, 01–03 are listed in Meyer and Bryan (1996); the whole rock composition for Sample 158-957B-4R-1, 55–62 cm, is given in Table 3. These parental liquid compositions are utilized in the modeling of the melting and fractional crystallization histories of the TAG region samples. FeO* = total iron as FeO.

Partial Melting Constraints on Major-Element Geochemistry

MORB most likely consist of hybridized melts formed during partial melting of adiabatically decompressing asthenosphere at spreading centers (e.g., Oxburgh and Turcotte, 1968; McKenzie, 1984; Klein and Langmuir, 1987). Fractional crystallization, magma mixing, and magma pooling affect basaltic melt packages during ascent and residence in crustal-level magma chambers.

The extent of partial melting in the upwelling asthenospheric mantle beneath a mid-ocean spreading center is thought to affect the Na_2O abundances and CaO/Al_2O_3 ratios of the basaltic liquids generated from it. As the extent of partial melting increases, Na_2O contents decrease while the CaO/Al_2O_3 ratios increase at similar extents of fractionation of the basaltic liquids. Increasing average pressures of partial melting may be correlated with higher FeO contents and lower SiO_2/FeO ratios (Klein and Langmuir, 1987; Niu and Batiza, 1991). Therefore, basaltic liquids that have been corrected for fractional crystallization to 8 wt% MgO with low Na_8 and high Ca_8/Al_8 and Fe_8 values would be predicted by Klein and Langmuir's model to have been formed by larger extents of partial melting and melting that extends to greater depths than samples with high Na_8 and low Ca_8/Al_8 and Fe_8 values. A general trend of increasing CaO/Al_2O_3 and decreasing Na_2O from the Kane/MARK region (~23°N) north to the Azores (~38°N) suggest that higher extents of partial melting in the mantle occur toward the Azores as shown in Figures 4A and 4B. However Shen and Forsyth (1995) have suggested that FeO (and Fe_8) is not a reliable indicator of the depth (or pressure) of melting. Variability in FeO contents in MORB may be a result of mantle source characteristics and volatile abundances rather than from fractional crystallization effects only (Shen and Forsyth, 1995).

The TAG region glasses and Leg 158 whole rocks display a range in CaO/Al_2O_3 ratios and Na_2O abundances in Figures 8A and 8B that can not be explained entirely by fractional crystallization of a single parental melt. The observed ranges in CaO/Al_2O_3 ratios and Na_2O abundances for a given MgO content then result from variations in parental melt compositions that may reflect variations in the composition of the mantle source region as well as variations in partial melting, mixing, and pooling processes discussed by Meyer and Bryan (1996) for the Mid-Atlantic Ridge glasses from the TAG segment. Since chemical heterogeneity in the mantle beneath the TAG region is not evident, chemical variations observed in erupted basalts likely reflect variations in melt generation and accumulation.

In order to estimate the degree of partial melting beneath the TAG segment, we have compared our calculated parental melts to those generated by Niu and Batiza (1991) in their decompression-induced column melting model. Niu and Batiza (1991) use a fertile mantle starting composition (MPY-90) which contains 0.40 wt% Na_2O. This model assumes that melting occurs continuously over a depth range (melting column) in response to the adiabatic rise of mantle material and that the melts efficiently segregate from the melting column, accumulating at the top. Mantle material at the top of the melting column therefore has undergone the highest degree of melting (Fmax). The pooled melt represents the sum of small batches of melt produced throughout the melting column and thus is not in equilibrium with the adjacent mantle. Figures 9A and 9B suggest that the maximum extent of melting in the mantle beneath TAG was between ~16% and ~25%, corresponding to a mean degree of melting over the entire melting column of ~8% to ~13% (Langmuir et al., 1993; Plank and Langmuir, 1992; Plank et al., 1995).

Trace- and Rare-Earth–Element Modeling

The modeling of trace-element and REE partial melting of typical depleted oceanic upper mantle is presented in this section for comparison with the major element modeling results, particularly for Na in

Table 7. Fractional crystallization modeling results for Leg 158 basalts.

	Model LLD-TAG-A calculated		Core, section, interval (cm) 957M-10R-1, 8-10 observed	Model LLD-TAG-C calculated		Core, section, interval (cm) 957B-4R-1, 55-62 observed
Pressure (kb)	6	4		6	4	
FLR	0.71	0.70		0.85	0.85	
Starting Temp (°C)	1314	1306		1422	1414	
Ending Temp (°C)	1228	1218		1258	1252	
SiO_2 (wt%)	50.88	50.99	51.10	50.35	50.33	50.26
TiO_2	1.42	1.43	1.55	1.62	1.62	1.62
Al_2O_3	15.65	15.59	15.34	15.22	15.20	15.14
FeO*	9.33	9.33	9.92	10.02	10.03	10.20
MgO	8.57	8.51	8.65	9.31	9.37	9.39
CaO	11.39	11.34	10.70	11.16	11.14	11.09
Na_2O	2.77	2.81	2.75	2.31	2.31	2.30
$100 \times (Mg/[Mg + Fe^{2+}])$	64.5	64.4	63.4	64.7	64.9	64.5
X(olivine)	0.31	0.31		1.00	1.00	
X(plagioclase)	0.69	0.69		0.00	0.00	
Equilibrium olivine	$Fo_{86.6}$	$Fo_{86.5}$	$Fo_{86.1}$	$Fo_{86.7}$	$Fo_{86.9}$	
Equilibrium plagioclase	$An_{70.1}$	$An_{71.3}$		$An_{74.7}$	$An_{76.3}$	

Notes: The calculated liquid compositions, crystallizing mineral phase proportions, and mineral compositions for the Leg 158 representative samples are obtained from the liquid line of descent program, "BASALT," from Weaver and Langmuir (1990). See Table 6 and text for explanation of fractional crystallization model types. FLR is the fraction of liquid remaining. X(olivine) and X(plagioclase) represent the proportions of mineral phases crystallized at that particular fraction of liquid remaining.

the previous section. REE, Sr, Zr, Na, and Ti abundances for model depleted upper mantle is listed in Table 8 and is represented by spinel lherzolite for which the major-element composition is assumed to be homogeneous. The depleted mantle has a light-REE-depleted pattern with La at 1.1× chondrite and 2.5× chondrite heavy REE abundances (Loubet et al., 1975) and is shown in Figure 10A. In a N-type MORB source mantle, Na_2O abundances are estimated to range from 0.26 wt% for an infertile source to 0.40 wt% for a fertile source (Kinzler and Grove, 1992a; Langmuir et al., 1993). The Na_2O content of the MARK mantle source region (Kane Transform region) has been estimated at 0.30 wt% (Casey, 1997). The Na_2O abundance for the model mantle used here is also 0.30 wt% (2226 ppm) unlike the model of Niu and Batiza (1991).

To model the behavior of trace elements during partial melting, we have used the "Continuous Melting" program of Xia (1995). This program models critical melting which assumes a small amount of melt is retained in the residue during each increment of melting (analogous to the dynamic melting model of Langmuir et al., 1977) and calculates the instantaneous and pooled liquid compositions produced by critical melting from spinel lherzolite. The calculations are based on equations of Shaw (1970), Maaløe (1982), and Sobolev and Shimizu (1992). In this model, 1% melt is retained in the residuum during melting (McKenzie, 1984; Daines and Richter, 1988). Partial melting is stopped at 25% which is prior to the disappearance of clinopyroxene in the model. The extents of melting calculated for the pooled liquids represent maximum extents (Fmax). The proportions of mineral phases in the starting assemblage for the spinel lherzolite (olivine, orthopyroxene, clinopyroxene, and spinel) and the melting proportions for these phases are listed in Table 8 and are the same as those used by Johnson et al. (1990). The mineral/liquid partition coefficients used in the trace element partial melting and fractional crystallization modeling are provided in Table 9.

The results of modeling critical melting of a depleted mantle are shown in Figure 10A with the predicted Sr, Zr, Na, Ti, and REE abundances for pooled melts generated by melting in the spinel stability field. As shown in Figure 6, the spidergrams of the Hole 957B and 957M whole rocks exhibit negative Ti and Sr anomalies and positive Zr anomalies. Partial melting of the model depleted mantle in the spinel stability field (10–25 kb) generates negative Ti anomalies and positive Zr anomalies in the pooled melts (Fig. 10A). Partial melting in the garnet stability field would generate positive Ti anomalies and no Zr anomalies in the pooled melts (Smith, 1994). Therefore, partial melting modeling involving garnet (at pressures > 25 kb) in garnet stability field is not required. Negative Sr anomalies however are not produced during melting (Fig. 10A) but rather are a consequence of fractionation crystallization of plagioclase. Samples TAG75-01B-21 and AII-129-5, 1–3 (Meyer and Bryan, 1996) and 158-957M-10R-1, 8–10 cm (this study), which represent the variability range in extents of melting (Fig. 9) are shown in Figures 10B and 10C with the estimated parental liquid and the daughter liquid spidergrams after fractional crystallization. From the trace-element and REE modeling, the predicted maximum extent of partial melting (Fmax) from the model depleted upper mantle for AII-129-5, 1–3 is ~25% (Fig. 10B) which is the same as the upper extent of melting estimated by major elements (Fig. 9). This parental pooled melt produced by 25% partial melting then undergoes moderate pressure (~6 kb) fractional crystallization to generate the daughter liquid (Fig. 10B). The Na anomaly in the daughter liquid does not correspond with the spidergram of AII-129-5, 1–3 for the given model source composition but could be matched using a more fertile source composition. The maximum extent of melting for TAG75-1B-21 is estimated at ~14%, which is slightly lower than the extent of melting predicted by the model of Niu and Batiza (1991). The spidergram of TAG75-1B-21 corresponds well with the calculated daughter liquid in which the predicted negative Sr and Na anomalies and positive Zr anomaly fit well with this glass composition (Fig. 10B). The maximum fraction of melting of the parental melt for representative sample 158-957M-10R-1, 8–10 cm, is ~11% (Fig. 10C), which corresponds to a value of ~6% for Fmean. This parental pooled melt produced by ~11% partial melting then undergoes moderate pressure (~6 kb) fractional crystallization to produce the daughter liquid. The spidergram of Sample 158-957M-10R-1, 8–10 cm, is well matched with the calculated daughter liquid. The predicted negative Sr, Na, and Ti anomalies and positive Zr anomaly correspond well with the representative whole-rock composition for Leg 158 basalts (Fig. 10C).

The range in maximum extents of partial melting based on major-, trace-, and rare-earth elements extends from ~11 to ~25%, but most of the TAG region basalts show compositions, which indicate predicted maximum extents of partial melting of less than 20%.

The range in extents of partial melting estimated for the TAG region is greater than those estimated for the MARK area at 23°N (Casey, 1997) and for the ridge segment south of the Hayes Transform at 33°N (Smith, 1994). Using similar methods to those applied here, Casey (1997) arrived at ~10% to ~15% partial melting (Fmax) for the MARK source region while Smith (1994) estimated ~20% partial melting (Fmax) for the southern Hayes source region. Basalts recovered from the Hayes Transform valley, however, show a large variation in the predicted extents of melting (~11% to ~22%) based on similar modeling (Smith, 1994) that is comparable to the melting range of the TAG segment basalts. Looking at the Mid-Atlantic

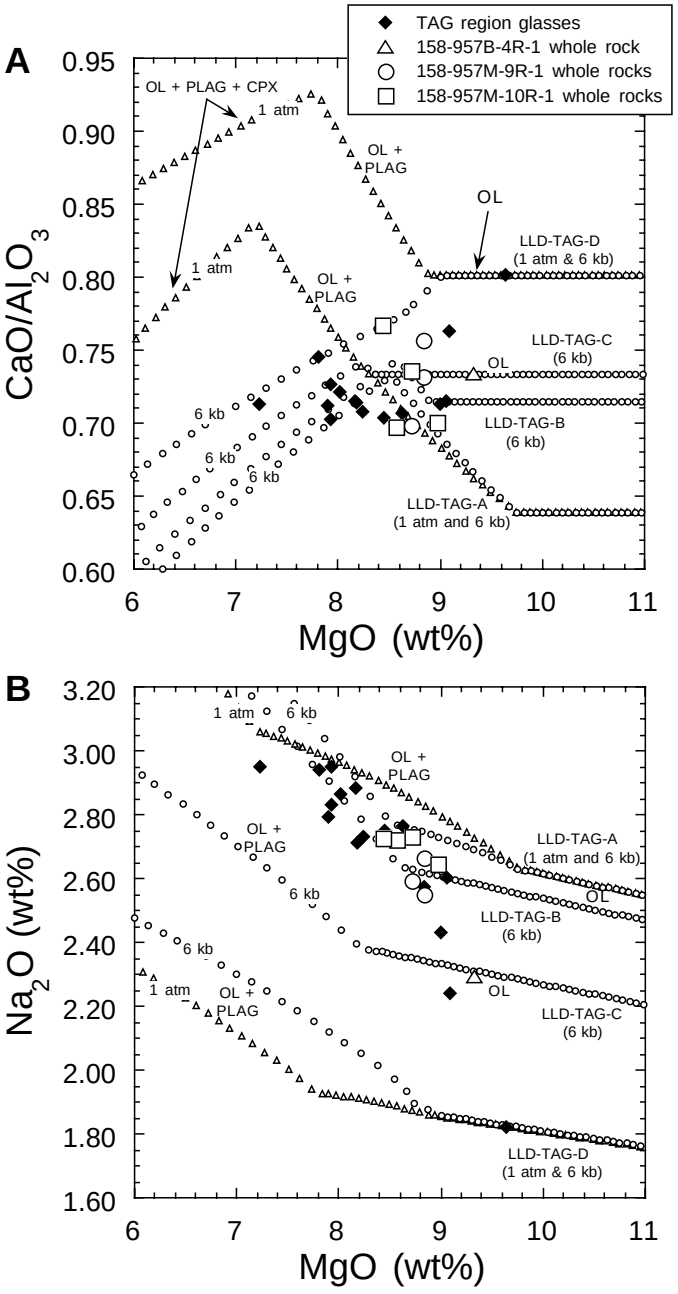

Figure 8. MgO (wt%) vs. CaO/Al_2O_3 (**A**) and MgO (wt%) vs. Na_2O (wt%) (**B**) variation diagrams for Leg 158 basaltic whole rocks (this study) and TAG region basaltic glasses from Meyer and Bryan (1996; rift valley and eastern wall samples only). Displayed in (A) and (B) are the calculated liquid lines of descent for fractional crystallization of calculated parental melts based on glass compositions of TAG75-01B-21 (LLD-TAG-A), TAG77-07-10 (LLD-TAG-B), and AII-129-5,01–03 (LLD-TAG-D) from Meyer and Bryan (1996) and on whole-rock composition of Sample 158-957B-4R-1, 55–62 cm, (LLD-TAG-C) for comparison (see Tables 6 and 7). The glass compositions have been back calculated to a starting composition of Mg-number ~71 where olivine in equilibrium with the liquid has the composition of Fo_{90} using the program "PETROLOG v. 1.0" by Danyushevsky (1991). LLD = liquid line of descent. Fractionating phases: OL = olivine; PLAG = plagioclase; and CPX = clinopyroxene. All liquid lines of descent for fractional crystallization are calculated utilizing the program "BASALT" from Weaver and Langmuir (1990) at pressures of 1 atm, 4 kb, and 6 kb.

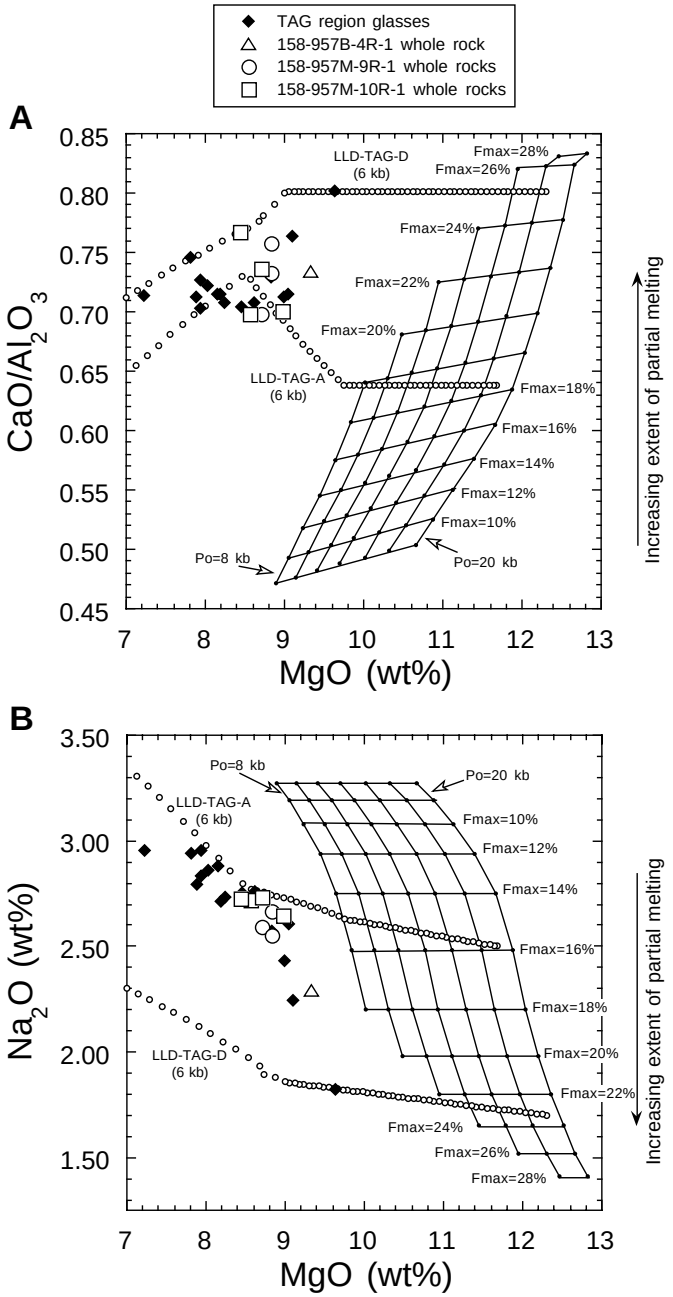

Figure 9. MgO (wt%) vs. CaO/Al_2O_3 (**A**) and MgO (wt%) vs. Na_2O (wt%) (**B**) variation diagrams for Leg 158 basaltic whole rocks (this study) and TAG region basaltic glasses from Meyer and Bryan (1996; rift valley and eastern wall samples only). The empirical estimates are shown for the extent of partial melting (f) from 6% to 28% and pressure of initial melting (P_o) from 8 kb to 20 kb in the source region from Niu and Batiza (1991). Displayed in (A) and (B) are the calculated liquid lines of descent for fractional crystallization of calculated parental melts based on glass compositions of TAG75-01B-21 (LLD-TAG-A) and AII-129-5, 01–03 (LLD-TAG-D) from Meyer and Bryan (1996) for comparison with the TAG region samples and the partial melting model of Niu and Batiza (1991).

Table 8. Model mantle source compositions for REEs, Sr, Zr, Na, and Ti, mantle phase proportions, and melting phase proportions.

Model depleted mantle spinel stability field partial melting	
La (ppm)	0.258
Ce	0.905
Sr	12.87
Nd	0.814
Na	2226
Zr	7.88
Sm	0.309
Eu	0.123
Gd	0.452
Ti	1046
Dy	0.607
Er	0.397
Yb	0.406

Spinel lherzolite phase	Initial proportion	Melting proportion
Olivine	0.55	0.10
Orthopyroxene	0.25	0.20
Clinopyroxene	0.18	0.68
Spinel	0.02	0.02

Notes: The starting bulk composition for the depleted mantle model has a light-REE-depleted pattern starting at 1.1x chondrite for La and 2.5x chondrite heavy-REE (Loubet et al., 1975) except for Na and Ti (Kinzler and Grove, 1992b). The starting composition is forward modeled to have experienced 25% partial melting in the spinel lherzolite facies (see Fig. 10A). The mantle phase and melting volume proportions for the spinel lherzolite assemblage are from Johnson et al. (1990).

Ridge as a whole, then, the maximum extent of melting decreases from 38°N at the Azores hot spot to 23°N at the Kane Transform (MARK region). The TAG region shows more variability in the melting and pooling regime than at the Kane Transform and south of the Hayes Transform based on the glasses from the TAG segment and the Leg 158 whole rocks.

CONCLUSIONS

The Leg 158 sample suite includes samples whose whole-rock chemical compositions have been altered by hydrothermal fluids associated with the TAG hydrothermal mineral deposit. These whole-rock compositions show decreasing SiO_2, CaO, Na_2O, and Sr contents and increasing Al_2O_3, Fe_2O_3, MgO, Cr, Zn, Y, and Zr contents as alteration progresses from fresh MORB to hydrothermal clay. whole-rock changes from the hydrothermal clay group to the metabasaltic clasts consist of decreasing Al_2O_3, MgO, CaO, Y, and Zr contents and increasing SiO_2, Fe_2O_3, Na_2O, Sr, and $(La/Sm)_{cn}$ values. Relatively unaltered basalts have Mg-numbers of 62.6–64.5, 0.70–0.77 CaO/Al_2O_3 ratios, 2.29–2.73 wt% Na_2O, 0.66–0.73 $(La/Sm)_{cn}$ ratios, and $Fo_{85.8}$–$Fo_{86.3}$ olivines. The Leg 158 basaltic whole-rock compositions are similar to the reported glass compositions from this region in major-, trace-, and rare-earth–element characteristics.

Fractional crystallization modeling using pseudoternary projections and liquid lines of descent calculations indicate that the Leg 158 basalts have experienced moderate pressure fractionation at 4 to 6 kb suggesting rapid ascent from the upper mantle and very short crustal residence times. The Leg 158 basalts have probably undergone olivine then olivine + plagioclase fractionation at 4 to 6 kb. Multiple parental melt compositions are indicated from major-element modeling for the Leg 158 and Mid-Atlantic Ridge glasses from the TAG region. Maximum extents of partial melting to produce these parental melts in the spinel stability field (10–25 kb) of the upper mantle show a range from ~11% to ~25% based on major-, trace-, and rare-earth–element modeling. The majority of the Leg 158 whole rocks and TAG region glasses, however, indicate derivation from the lower end of the melting range (<20%), which spans the range of the MARK samples from Leg 153 (~10% to ~15%) and Hayes Transform region basalts (~20%). South from the Azores hotspot region, the extents of partial melting show an overall decline as the TAG region at 26°N and the MARK area at 23°N are approached, but melt production and accumulation processes along the TAG segment provide variability on the local scale.

ACKNOWLEDGMENTS

The authors would like to express their gratitude to the captain and crew of the Leg 158 *JOIDES Resolution* cruise. We would like to thank Michael Dix for his assistance in the ICP laboratory at the University of Houston. We also like to thank Milton Pierson for his assistance in the electron microprobe facility at Rice University. This manuscript has been greatly improved by the constructive comments of Rodey Batiza, Peter Meyer, and Michael Perfit. This research has been supported by JOI/USSAC.

REFERENCES

Allègre, C.J., and Turcotte, D.L., 1986. Implications of a two-component marble-cake mantle. *Nature*, 323:123–127.

Anders, E., and Grevesse, N., 1989. Abundances of the elements: meteoritic and solar. *Geochim. Cosmochim. Acta*, 53:197–214.

Bougault, H., Joron, J.L., Treuil, M., and Maury, R., 1985. Local versus regional mantle heterogeneities: evidence form hygromagmaphile elements. *In* Bougault, H., and Cande, S.C., et al., *Init. Repts. DSDP*, 82: Washington (U.S. Govt. Printing Office), 459–482.

Brannon, J.C., 1985. The degree of heterogeneity in basalts near the Hayes Fracture Zone, Mid-Atlantic Ridge: Holes 561, 562, and 564. *In* Bougault, H., and Cande, S.C., et al., *Init. Repts. DSDP*, 82: Washington (U.S. Govt. Printing Office), 439–447.

Bryan, W.B., Humphris, S.E., Thompson, G., and Casey, J.F., 1994. Comparative volcanology of small axial eruptive centers in the MARK area. *J. Geophys. Res.*, 99:2973–2984.

Bryan, W.B., Thompson, G., Frey, F.A., and Dickey, J.S., 1976. Inferred settings and differentiation in basalts from the Deep Sea Drilling Project. *J. Geophys. Res.*, 81:4285–4304.

Casey, J.F., 1997. Comparison of major- and trace-element geochemistry of abyssal peridotites and mafic plutonic rocks with basalts from the MARK region of the Mid-Atlantic Ridge. *In* Karson, J.A., Cannat, M., Miller, D.J., and Elthon, D. (Eds.), *Proc. ODP, Sci. Results*, 153: College Station, TX (Ocean Drilling Program), 181–241.

Cohen, R.S., and O'Nions, R.K., 1982. The lead, neodynium and strontium isotopic structure of ocean ridge basalts. *J. Petrol.*, 23:299–324.

Daines, M.J., and Richter, F.M., 1988. An experimental method for directly determining the interconnectivity of melt in a partially molten system. *Geophys. Res. Lett.*, 15:1459–1462.

Danyushevsky, L.V., 1991. Petrology and geochemistry of the Tonga boninites [Ph.D. dissert.]. Vernadsky Inst. of Geochemistry and Analytical Chemistry, Moscow.

DePaolo, D.J., and Wasserburg, G.J., 1976a. Inferences about magma sources and mantle structures from variations in $^{143}Nd/^{144}Nd$. *Geophys. Res. Lett.*, 3:743–746.

————, 1976b. Nd isotopic variations and petrogenetic models. *Geophys. Res. Lett.*, 3:249–252.

Dick, H.J.B., and Kelemen, P.B., 1991. Fractionation of Ti from rare earth elements during formation of harzburgite from lherzolite by magma/mantle interaction. *Eos*, 72:545.

Dmitriev, L.V., Magakian, R., Daniushevky, L.V., Kamenetsky, V.S., and Kononkova, N.N., 1991. New data on primitive tholeiites from oceanic crust of the Atlantic (from materials of Cruise 12 of R/V *Academician B. Petrov*). *Volcanol. Seismol.*, 6:78–94. (in Russian)

Dmitriev, L.V., Sobolev, A.V., Suschevskaya, N.M., and Zapunny, S.A., 1985. Abyssal glasses, petrologic mapping of the oceanic floor and "Geochemical Leg 82." *In* Bougault, H., and Cande, S.C., et al., *Init. Repts. DSDP*, 82: Washington (U.S. Govt. Printing Office), 509–518.

Drake, N.E.R., Rhodes, J.M., and Autio, L.K., 1985. The geochemistry of the Leg 82 Basalts. *In* Bougault, H., Cande, S.C., et al., *Init. Repts. DSDP*, 82: Washington (U.S. Govt. Printing Office), 421–438.

Dungan, M.A., Rhodes, J.M., Long, P.E., Blanchard, D.P., Brannon, J.C., and Rodgers, K.V., 1978. The petrology and geochemistry of basalts from

Site 396, Legs 45 and 46 of the Deep Sea Drilling Project. *In* Dmitriev, L.V., Heirtzler, J., et al., *Init. Repts. DSDP,* 46: Washington (U.S. Govt. Printing Office), 89–113.

Dupré, B., Göpel, C., and Bougault, H., 1985. Lead isotopic variations in old ocean crust near the Azores. *In* Bougault, H., and Cande, S.C., et al., *Init. Repts. DSDP,* 82: Washington (U.S. Govt. Printing Office), 497–500.

Frey, F.A., Walker, N., Stakes, D., Hart, S.R., and Nielsen, R., 1993. Geochemical characteristics of basaltic glasses from the AMAR and FAMOUS axial valleys, Mid-Atlantic Ridge (36°–37°N): petrogenetic implications. *Earth Planet. Sci. Lett.,* 115:117–136.

Fujimaki, H., Tatsumoto, M., and Aoki, K., 1984. Partition coefficients of Hf, Zr, and REE between phenocrysts and groundmasses. *Proc. Lunar Planet. Sci. Conf., 14th (Part 2).* J. Geophys. Res., 89 (Suppl.):B662–B672.

Grove, T.L., Kinzler, R.J., and Bryan, W.B., 1992. Fractionation of mid-ocean ridge basalt (MORB). *In* Morgan, J.P., Blackman, D.K., and Sinton, J.M. (Eds.), *Mantle Flow and Melt Generation at Mid-Ocean Ridges.* Geophys. Monogr., Am. Geophys. Union, 71:281–310.

Hamelin, B., Dupré, B., and Allègre, C.J., 1984. Lead-strontium isotopic variations along the East Pacific Rise and the Mid-Atlantic Ridge: a comparative study. *Earth Planet. Sci. Lett.,* 67:340–350.

Hart, S.R., and Dunn, T., 1993. Experimental CPX/melt partitioning of 24 trace elements. *Contrib. Mineral. Petrol.,* 113:1–8.

Hertogen, J., Sachtleben, T., Schmincke, H.U., and Jenner, G.A., 1985. Trace element geochemistry and petrogenesis of basalts from Deep Sea Drilling Project Sites 556–559 and 561–564. *In* Bougault, H., and Cande, S.C., et al., *Init. Repts. DSDP,* 82: Washington (U.S. Govt. Printing Office), 449–457.

Hess, P.C., 1992. Phase equilibria constraints on the origin of ocean floor basalts. *In* Phipps Morgan, J., Blackman, D.K., and Sinton, J.M. (Eds.), *Mantle Flow and Melt Generation at Mid-Ocean Ridges.* Geophys. Monogr., Am. Geophys. Union, 71:67–102.

Humphris, S.E., Bryan, W.B., Thompson, G., and Autio, L.K., 1990. Morphology, geochemistry, and evolution of Serocki volcano. *In* Detrick, R., Honnorez, J., Bryan, W.B., Juteau, T., et al. *Proc. ODP, Sci. Results,* 106/109: College Station, TX (Ocean Drilling Program), 67–84.

Humphris, S.E., Herzig, P.M., Miller, D.J., et al., 1996. *Proc. ODP, Init. Repts.,* 158: College Station, TX (Ocean Drilling Program).

Humphris, S.E., Kleinrock, M.C., and the Deep-TAG Team, 1994. Detailed morphology and the distribution of venting at the active TAG hydrothermal mound, 26°N, Mid-Atlantic Ridge. *Eos,* 75:660.

Irving, A.J., 1978. A review of experimental studies of crystal/liquid trace element partitioning. *Geochim. Cosmochim. Acta,* 42:743–770.

Ito, E., White, W.M., and Göpel, C., 1987. The O, Sr, Nd and Pb isotope geochemistry of MORB. *Chem. Geol.,* 62:157–176.

Jenner, G.A., Hertogen, J., Sachtleben, T., and Schmincke, H.-U., 1985. Isotopic and trace element composition of basalts from Sites 556–559 and 561–564: constraints on some processes affecting their composition. *In* Bougault, H., and Cande, S.C., et al., *Init. Repts. DSDP,* 82: Washington (U.S. Govt. Printing Office), 501–507.

Johnson, K.T.M., Dick, H.J.B., and Shimizu, N., 1990. Melting in the oceanic upper mantle: an ion microprobe study of diopsides in abyssal peridotites. *J. Geophys. Res.,* 95:2661–2678.

Kelemen, P.B., Shimizu, N., and Dunn, T., 1993. Relative depletion of niobium in some arc magmas and the continental crust: partitioning of K, Nb, La, and Ce during melt/rock reaction in the upper mantle. *Earth Planet. Sci. Lett.,* 120:111–133.

Kinzler, R.J., and Grove, T.L., 1992a. Primary magmas of mid-ocean ridge basalts, 1. Experiments and methods. *J. Geophys. Res.,* 97:6885–6906.

————, 1992b. Primary magmas of mid-ocean ridge basalts, 2. Applications. *J. Geophys. Res.,* 97:6907–6926.

Klein, E.M., and Langmuir, C.H., 1987. Global correlations of ocean ridge basalt chemistry with axial depth and crustal thickness. *J. Geophys. Res.,* 92:8089–8115.

————, 1989. Local versus global variations in ocean ridge basalt composition: a reply. *J. Geophys. Res.,* 94:4241–4252.

Langmuir, C.H., Bender, J.F., Bence, A.E., and Hanson, G.N., 1977. Petrogenesis of basalts from the FAMOUS area: Mid-Atlantic Ridge. *Earth Planet. Sci. Lett.,* 36:133–156.

Langmuir, C.H., Klein, E., and Plank, T., 1993. Petrological systematics of mid-ocean ridge basalts: constraints on melt generation beneath ocean ridges. *In* Morgan, J., Blackman, D., Sinton, J. (Eds.), *Mantle Flow and Melt Generation at Mid-Ocean Ridges.* Geophys. Monogr., Am. Geophys. Union, 71:183–277.

Loubet, M., Shimizu, N., and Allègre, C.J., 1975. Rare earth elements in alpine peridotites. *Contrib. Mineral. Petrol.,* 53:1–12.

Maaloe, S., 1982. Geochemical aspects of permeability controlled partial melting and fractional crystallization. *Geochim. Cosmochim. Acta,* 46:43–57.

McDonough, W.F., and Frey, F.A., 1989. Rare earth elements in upper mantle rocks. *In* Lipin, B.R., and McKay, G.A. (Eds.), *Geochemistry and Mineralogy of Rare Earth Elements.* Rev. Mineral., 21:99–145.

McKay, G.A., 1986. Crystal/liquid partitioning of REE in basaltic systems: extreme fractionation of REE in olivine. *Geochim. Cosmochim. Acta,* 50:69–79.

McKenzie, D., 1984. The generation and compaction of partially molten rock. *J. Petrol.,* 25:713–765.

McLennan, S.M., 1989. Rare earth elements in sedimentary rocks: influence of provenance and sedimentary processes. *In* Lipin, B.R., and McKay, G.A. (Eds.), *Geochemistry and Mineralogy of the Rare Earth Elements.* Rev. Mineral., 21:169–200.

Meaux, D.P., 1989. Geology and geochemistry of subophiolitic volcanic rocks in the Humber Arm Allocthon, western Newfoundland, Canada. [M.S. thesis]. Univ. of Houston, TX.

Melson, W.G., and O'Hearn, T., 1986. "Zero-age" variations in the compositions of abyssal volcanic rocks along the axial zone of the Mid-Atlantic ridge. *In* Vogt, P.R., and Tucholke, B.E. (Eds.), *The Geology of North America* (Vol. M): *The Western North Atlantic Region.* Geol. Soc. Am., 17–136.

Meyer, P.S., and Bryan, W.B., 1996. Petrology of basaltic glasses from the TAG segment: implications for a deep hydrothermal heat source. *Geophys. Res. Lett.,* 23:3435–3438.

Niu, Y., and Batiza, R., 1991. An empirical method for calculating melt compositions produced beneath mid-ocean ridges: application for axis and off-axis (seamounts) melting. *J. Geophys. Res.,* 96:21753–21777.

O'Donnell, T.H., and Presnall, D.C., 1980. Chemical variations of the glass and mineral phases in basalts dredged from 25-30°N along the mid-Atlantic ridge. *Am. J. Sci.,* 280A:845–868.

Oxburgh, E.R., and Turcotte, D.L., 1968. Mid-ocean ridges and geotherm distribution during mantle convection. *J. Geophys. Res.,* 73:2643–2661.

Pearce, J.A., and Parkinson, I.J., 1993. Trace element models for mantle melting: application to volcanic arc petrogenesis. *In* Pritchard, H.M., Alabaster, T., Harris, N.B.W., and Neary, C.R. (Eds.), *Magmatic Processes and Plate Tectonics.* Geol. Soc. Spec. Publ. London, 76:373–403.

Phinney, W.C., and Morrison, D.A., 1990. Partition coefficients for calcic plagioclase: implications for Archean anorthosites. *Geochim. Cosmochim. Acta,* 54:1639–1654.

Plank, T., and Langmuir, C.H., 1992. Effects of the melting regime on the composition of the oceanic crust. *J. Geophys. Res.,* 97:19749–19770.

Plank, T., Spiegelman, M., Langmuir, C.H., and Forsyth, D.W., 1995. The meaning of "mean F": clarifying the mean extent of melting at ocean ridges. *J. Geophys. Res,* 100:15045–15052.

Pouchou, J.L., and Pichoir, F., 1985. "PAP" f(r[0122S]) procedure for improved quantitative microanalysis. *In* Armstrong, J.T. (Ed.), *Microbeam Analysis:* (San Francisco Press), 104–106.

Prinzhofer, A., Lewin, E., and Allègre, C.J., 1989. Stochastic melting of the marble cake mantle: evidence from local study of the East Pacific Rise at 12°50′N. *Earth Planet. Sci. Lett.,* 92:189–206.

Purdy, G.M., Sempéré, J.-C., Schouten, H., Dubois, D.L., and Goldsmith, R., 1990. Bathymetry of the Mid-Atlantic Ridge, 24°–31°N: a map series. *Mar. Geophys. Res.,* 12:247–252.

Rideout, M.L., and Schilling, J.-G., 1985. Rare-earth elements, $^{87}Sr/^{86}Sr$, and $^{143}Nd/^{144}Nd$ mantle source variations. *In* Bougault, H., and Cande, S.C., et al., *Init. Repts. DSDP,* 82: Washington (U.S. Govt. Printing Office), 483–496.

Roeder, P.L., and Emslie, R.F., 1970. Olivine-liquid equilibrium. *Contrib. Mineral. Petrol.,* 29:275–289.

Rona, P.A., Harbison, R.N., Bassinger, B., Scott, R.B., and Nalwalk, A.J., 1976. Tectonic fabric and hydrothermal activity of Mid-Atlantic Ridge crest (26°N latitude). *Geol. Soc. Am. Bull.,* 87:661–674.

Sato, H., Aoki, K.I., Okamoto, K., and Fujita, B., 1979. Petrology and chemistry of basaltic rocks from the Hole 396B, IPOD/DSDP Leg 46. *In* Dmitriev, L., Heirtzler, J., et al., *Init. Repts. DSDP,* 46: Washington (U.S. Govt. Printing Office), 115–141.

Schilling, J.-G., 1975. Rare-earth variations across "normal segments" of the Reykjanes Ridge, 60°–53°N, Mid-Atlantic Ridge, 29°S, and East Pacific Rise, 2°–19°S, and evidence on the composition of the underlying low-velocity layer. *J. Geophys. Res.,* 80:1459–1473.

Schilling, J.-G., Zajac, M., Evans, R., Johnston, T., White, W., Devine, J.D., and Kingsley, R., 1983. Petrologic and geochemical variations along the Mid-Atlantic ridge from 29°N to 73°N. *Am. J. Sci.*, 283:510–586.

Sempéré, J.-C., Purdy, G.M., and Schouten, H., 1990. Segmentation of the Mid-Atlantic Ridge between 24°N and 30°40´N. *Nature*, 344:427–431.

Shaw, D.M., 1970. Trace element fractionation during anantexis. *Geochim. Cosmochim. Acta*, 34:237–243.

Shen, Y., and Forsyth, D.W., 1995. Geochemical constraints on initial and final depths of melting beneath mid-ocean ridges. *J. Geophys. Res.*, 100:2211–2237.

Shibata, T., and Fox, P.J., 1975. Fractionation of abyssal tholeiites: samples from the Oceanographer Fracture Zone (35°N, 35°W). *Earth Planet. Sci. Lett.*, 27:62–72.

Sigurdsson, H., 1981. First-order major element variation in basalt glasses from the Mid-Atlantic Ridge: 29°N to 73°N. *J. Geophys. Res.*, 86:9483–9502.

Smith, D.R., and Cann, J.R., 1992. The role of seamount volcanism in crustal construction at the Mid-Atlantic Ridge (24°–30°N). *J. Geophys. Res.*, 97:1645–1658.

Smith, S.E., 1994. Geochemistry and petrology of basaltic and plutonic rocks from the Hayes Transform Region, Mid-Atlantic Ridge [Ph.D. dissert.]. Univ. of Houston, Houston, TX.

Sobolev, A.V., and Shimizu, N., 1992. Ultra-depleted melts and permeability of the oceanic mantle. *Dokl. Acad. Sci. Russia*, 236:354–360. (in Russian)

Stakes, D.S., Shervais, J.W., and Hopson, C.A., 1984. The volcanic-tectonic cycle of the FAMOUS and AMAR valleys, Mid-Atlantic Ridge (36°47´N): evidence from basalt glass and phenocryst compositional variations for a steady state magma chamber beneath the valley mid-sections, AMAR 3. *J. Geophys. Res.*, 89:6995–7028.

Stosch, H.-G., 1982. Rare earth element partitioning between minerals from anhydrous spinel peridotite xenoliths. *Geochim. Cosmochim. Acta*, 46:793–811.

Sun, S.-S., and McDonough, W.F., 1989. Chemical and isotopic systematics of oceanic basalts: implications for mantle composition and processes. *In* Saunders, A.D., and Norry, M.J. (Eds.), *Magmatism in the Ocean Basins.* Geol. Soc. Spec. Publ. London, 42:313–345.

Sun, S.-S., Nesbitt, R.W., and Sharaskin, A.Y., 1979. Geochemical characteristics of mid-ocean ridge basalts. *Earth Planet. Sci. Lett.*, 44:119–138.

Tarney, J., Saunders, A.D., Weaver, S.D., Donnellan, N.C.B., and Hendry, G.L., 1979. Minor element geochemistry of basalts from Leg 49, North Atlantic Ocean. *In* Luyendyk, B.P., Cann, J.R., et al., *Init. Repts. DSDP*, 49: Washington (U.S. Govt. Printing Office), 657–691.

Weaver, B.L., Tarney, J., and Saunders, A.D., 1985. Geochemistry and mineralogy of basalts recovered from the Central North Atlantic. *In* Bougault, H., and Cande, S.C., et al., *Init. Repts. DSDP*, 82: Washington (U.S. Govt. Printing Office), 395–419.

Weaver, J.S., and Langmuir, C.H., 1990. Calculation of phase equilibrium in mineral-melt systems. *Comput. Geosci.*, 16:1–19.

Weill, D.F., and McKay, G.A., 1975. The partitioning of Mg, Fe, Sr, Ce, Sm, Eu, and Yb in lunar igneous systems and a possible origin of KREEP by equilibrium partial melting. *Proc. 6th Lunar Sci. Conf.*, 1143–1158.

White, W.M., and Bryan, W.B., 1977. Sr-isotope, K, Rb, Cs, Sr, Ba, and rare-earth geochemistry of basalts from the FAMOUS area. *Geol. Soc. Am. Bull.*, 88:571–576.

White, W.M., and Hofmann, A.W., 1982. Sr and Nd isotope geochemistry of oceanic basalts and mantle evolution. *Nature*, 296:821–825.

White, W.M., and Schilling, J-G., 1978. The nature and origin of geochemical variation in Mid-Atlantic Ridge basalts from the central north Atlantic. *Geochim. Cosmochim. Acta*, 42:1501–1516.

Xia, C., 1995. Geochemistry and petrogenesis of mid-ocean ridge basalts from 12°–16°N, Mid-Atlantic Ridge [Ph.D. dissert.]. Univ. of Houston, TX.

Zindler, A., Jagoutz, E., and Goldstein, S., 1982. Nd, Sr and Pb isotopic systematics in a three-component mantle: a new perspective. *Nature*, 298:519–523.

Date of initial receipt: 29 May 1996
Date of acceptance: 31 December 1996
Ms 158SR-218

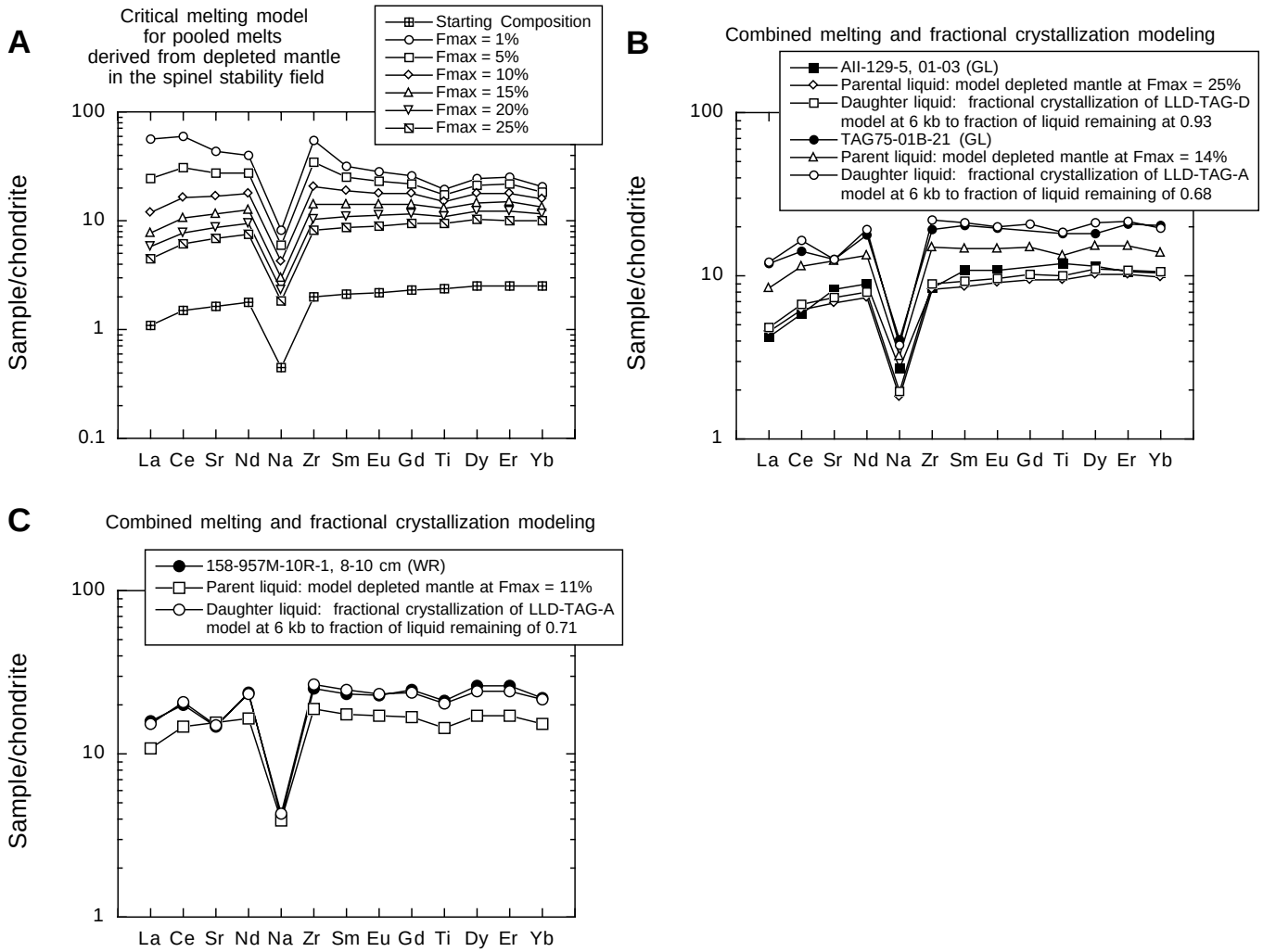

Figure 10. **A.** Spidergram of the pooled melts produced during critical melting of the model depleted mantle. Partial melting continues to a maximum extent (Fmax) of 25% in the spinel lherzolite field (<25 kb). Initial mantle trace-element compositions are given in Table 8 with spinel lherzolite phase proportions and melting proportions. The partition coefficients used in this modeling are given in Table 9. Partial melting pooled melts are calculated by the program, "Continuous Melting," by Xia (1995). **B.** Spidergram of AII-129-5, 01–03 and TAG75-01B-21 from Meyer and Bryan (1996) with modeling of parental pooled liquids derived from the model depleted mantle. For AII-129-5, 01–03, Fmax is 25% and LLD-TAG-D model is used to determine the daughter liquid composition at a fraction of liquid remaining of 0.93 at 6 kb. For TAG75-01B-21, Fmax is 14% and LLD-TAG-A model is used to determine the daughter liquid composition at a fraction of liquid remaining of 0.68 at 6 kb. **C.** Spidergram of Sample 158-957M-10R-1, 8–10 cm, with modeling of a parental pooled liquid (Fmax = 11%) derived from the model depleted mantle. The daughter liquid pattern produced from fractional crystallization of the parental liquid (model LLD-TAG-A) to a fraction of liquid remaining of 0.71 at 6 kb is displayed for comparison. Element incompatibility order from Pearce and Parkinson (1993). Chondrite normalization values from Anders and Grevesse (1989). GL = glass; WR = whole rock.

Table 9. Mineral/liquid partition coefficients used in major-, trace-, and rare-earth–element partial melting and fractional crystallization modeling.

	Olivine	Orthopyroxene	Clinopyroxene	Spinel	Plagioclase
Na_2O* (cpm)	0.0010	0.0400	0.2000	0.0010	1.0000
Na_2O* (pfx)	0.0010	0.0400	0.1500	0.0010	1.0000
Sr	0.0030	0.0180	0.1283	0.0001‡	1.6100
Zr	0.0005	0.0140	0.1234	0.0700	0.0094
Ti	0.0150	0.1400	0.3840	0.1500	0.0100‡
La	0.000007	0.0005	0.0536	0.0006	0.0415
Ce	0.00001	0.0009	0.0858	0.0006	0.0297
Nd	0.00007	0.0090	0.1873	0.0006	0.0230†
Sm	0.0007	0.0200	0.2910	0.0006	0.0177
Eu	0.00095	0.0300	0.3500	0.0006	0.1680
Gd	0.0012	0.0400	0.4000	0.0006	0.0120†
Dy	0.0040	0.0600	0.4420	0.0015	0.0090†
Er	0.0090	0.0700	0.3870	0.0030	0.0079†
Yb	0.0230	0.1000	0.4300	0.0045	0.0070

Notes: Olivine: McKay (1986); Kelemen et al. (1993) and references cited within; Irving (1978) and references cited within; Kinzler and Grove (1992a). Orthopyroxene: Kelemen et al. (1993) and references cited within; Dick and Kelemen (1991); Irving (1978) and references cited within; Weill and McKay (1975); Kinzler and Grove (1992a). Clinopyroxene: Hart and Dunn (1993); Kelemen et al. (1993); Kinzler and Grove (1992a). Spinel: Stosch (1982); Kelemen et al. (1993) and references cited within; Irving (1978) and references cited within; Kinzler and Grove (1992a). Plagioclase: Phinney and Morrison (1990); Fujimaki et al. (1984); Kinzler and Grove (1992a). For Na_2O*, different mineral/liquid partition coefficients are used for clinopyroxene during critical partial melting (cpm) at >9 kb and fractional crystallization (pfx) at <9 kb based on Kinzler and Grove (1992a). † = interpolated values from Phinney and Morrison (1990). ‡ = estimated value.